



Benzofuranyl-2-imidazoles as imidazoline I₂ receptor ligands for Alzheimer's disease



Sergio Rodríguez-Arévalo ^{a,1}, Andrea Bagán ^a, Christian Griñán-Ferré ^{b,1}, Foteini Vasilopoulou ^b, Mercè Pallàs ^b, Iria Brocos-Mosquera ^{c,d}, Luis F. Callado ^{c,d}, M. Isabel Loza ^e, Antón L. Martínez ^e, José Brea ^e, Belén Pérez ^f, Elies Molins ^g, Steven De Jonghe ^h, Dirk Daelemans ^h, Milica Radan ⁱ, Teodora Djikic ⁱ, Katarina Nikolic ⁱ, Elena Hernández-Hernández ^j, M. Julia García-Fuster ^j, Jesús A. García-Sevilla ^j, Carmen Escolano ^{a,*}

^a Laboratory of Medicinal Chemistry (Associated Unit to CSIC), Department of Pharmacology, Toxicology and Medicinal Chemistry, Faculty of Pharmacy and Food Sciences, Institute of Biomedicine (IBUB), University of Barcelona, Av. Joan XXIII, 27-31, E-08028, Barcelona, Spain

^b Pharmacology Section, Toxicology and Medicinal Chemistry, Faculty of Pharmacy and Food Sciences, Institut de Neurociències, University of Barcelona, Av. Joan XXIII, 27-31, E-08028, Barcelona, Spain

^c Department of Pharmacology, University of the Basque Country, UPV/EHU, E-48940, Leioa, Bizkaia, Spain

^d Centro de Investigación Biomédica en Red de Salud Mental, CIBERSAM, Spain

^e Innopharma Screening Platform, BioFarma Research Group, Centro de Investigación en Medicina Molecular y Enfermedades Crónicas (CIMUS), Universidad de Santiago de Compostela, E-15782, Santiago de Compostela, Spain

^f Department of Pharmacology, Therapeutic and Toxicology, Autonomous University of Barcelona, E-08193, Cerdanyola, Spain

^g Institut de Ciència de Materials de Barcelona (CSIC), Campus UAB, E-08193, Cerdanyola, Spain

^h KU Leuven, Department of Microbiology, Immunology and Transplantation, Rega Institute, Laboratory of Virology and Chemotherapy, Herestraat 49, 3000, Leuven, Belgium

ⁱ Department of Pharmaceutical Chemistry, Faculty of Pharmacy, University of Belgrade, 11000, Belgrade, Serbia

^j IUNICS University of the Balearic Islands (UIB), Health Research Institute of the Balearic Islands (IdISBa), E-07122, Palma de Mallorca, Spain

ARTICLE INFO

Article history:

Received 23 February 2021

Received in revised form

26 April 2021

Accepted 10 May 2021

Available online 20 May 2021

Keywords:

Imidazoline I₂ receptors

Imidazoline I₂ receptor ligands

Neuroprotection

5xFAD

Benzofuranyl-2-imidazoles

Oxidative stress

ABSTRACT

Recent findings unveil the pharmacological modulation of imidazoline I₂ receptors (I₂-IR) as a novel strategy to face unmet medical neurodegenerative diseases. In this work, we report the chemical characterization, three-dimensional quantitative structure-activity relationship (3D-QSAR) and ADMET *in silico* of a family of benzofuranyl-2-imidazoles that exhibit affinity against human brain I₂-IR and most of them have been predicted to be brain permeable. Acute treatment in mice with 2-(2-benzofuranyl)-2-imidazole, known as **LSL60101** (garsevil), showed non-warming properties in the ADMET studies and an optimal pharmacokinetic profile. Moreover, LSL60101 induced hypothermia in mice while decreased pro-apoptotic FADD protein in the hippocampus. *In vivo* studies in the familial Alzheimer's disease 5xFAD murine model with the representative compound, revealed significant decreases in the protein expression levels of antioxidant enzymes superoxide dismutase and glutathione peroxidase in hippocampus. Overall, **LSL60101** plays a neuroprotective role by reducing apoptosis and modulating oxidative stress.

© 2021 The Authors. Published by Elsevier Masson SAS. This is an open access article under the CC BY license (<http://creativecommons.org/licenses/by/4.0/>).

1. Introduction

Imidazoline I₂ receptors (I₂-IR) are heterogeneous entities, often described as nonadrenergic binding sites for imidazolines [1], that

bind with high affinity to [³H]idazoxan and with lower affinity to [³H]*p*-aminoclonidine and [³H]clonidine [2,3]. I₂-IR are present in many organs, tissues and cell types, including brain, kidney, liver, astrocytes, platelets [4], pancreatic cells and, vascular smooth muscle cells [5]. Modifications in the levels of I₂-IR have been associated with analgesia [6], inflammation [7] and with human brain disorders [8] such as depression [9], Alzheimer's type

* Corresponding author.

E-mail address: cescolano@ub.edu (C. Escolano).

¹ Both authors contribute equally to this work.

dementia [10], Parkinson's disease [11], and glial tumors [12]. The fact that I₂-IR are altered in many pathophysiological processes and the availability of known I₂-IR ligands have permitted to place I₂-IR in a privileged position as new promising therapeutic targets. Representative I₂-IR ligands [13] emerged from the literature as useful tools to reveal the biological implications of these non-structurally described receptors (Fig. 1). The compelling evidence has demonstrated the neuroprotective role of I₂-IR through the pharmacological activities observed for their ligands. Agmatine, identified as the endogenous I₂-IR ligand, has modulated actions in several neurotransmitters leading to neuroprotection in both *in vitro* and in rodent models [14]. Idazoxan reduced neuron damage in the rat brain hippocampus after global ischemia [15]. 2-(2-Benzofuranyl)-2-imidazoline (2-BFI), a selective I₂-IR ligand, provided neuroprotective benefits against cerebral ischemia in models of chronic opioid therapy [16]. Idazoxan and 2-BFI have been proposed to exert neuroprotection by direct blocking of N-methyl-D-aspartate receptor (NMDA) mediated intracellular [Ca²⁺] influx [17].

Two out of these seven ligands depicted in Fig. 1, CR4056 and [¹¹C]BU99008, are in the process of validating their therapeutic potential by progressing in clinical trials for osteoarthritis [18], and for PET diagnosis for patients that suffer from Alzheimer's disease (AD) [19,20], respectively. Due to the clinical implications of I₂-IR, the discovery of new I₂-IR ligands that could modulate the pharmacology involved is a challenging goal for a medicinal chemistry program. In this framework, we recently provided two structurally new families of I₂-IR ligands and validated their properties ameliorating the devastating cognitive decline in two murine models of neurodegeneration [21–23].

At the subcellular level in the central nervous system (CNS), I₂-IR are mainly located on the outer membrane of mitochondria in astrocytes [24,25]. Mitochondria are one of the main sources of reactive oxygen species (ROS) and reactive nitrogen species (RNS).

The amyloid cascade hypothesis, that dominates the field of AD, has been replaced by alternative explanations arising from the connection of mitochondrial dysfunction and increased ROS. There is evidence that indicates a pro-oxidant ability of Aβ, mediating an accelerated production of ROS by directly binding to the mitochondrial membranes. Consequently, mitochondrial dynamics and function are altered, disrupting the energy metabolism, and leading to the loss of synaptic function. An excess in ROS/RNS production and a mitochondrial dysfunction could lead to oxidative stress (OS), which is implicated in several neurodegenerative diseases, such as AD [26–28]. In fact, there is growing evidence for the contribution of OS and neuroinflammation to the pathogenesis of AD [29,30]. Recent studies have investigated the role of I₂-IR in OS processes. Selective 2-BFI [31] decreased OS and altered the levels of antioxidant enzymes in an AD rat model and protected against OS-induced astrocytic cell death. Moreover, our group reported decreased levels of hydrogen peroxide levels and OS markers induced by two new I₂-IR ligands in aged SAMP8 mice [32].

In this manuscript, we focused our attention on 2-(2-benzofuranyl)-2-imidazole, named as **LSL60101** (garsevil), first described in 1995 by García-Sevilla's group as a I₂-IR selective ligand involved in astrocyte activation and neuronal regeneration [33,34]. In the following years, some outstanding papers described the biological relevance of **LSL60101** in the attenuation of morphine tolerance and hence proposing a neuroprotective role [35], such as provoking morphological/biochemical changes in astroglia that were neuroprotective after neonatal axotomy [36], and producing discriminable stimulus [37], amongst others. Of note, astrocytes as the main supportive cells in the CNS are significantly involved in the redox homeostasis, and consequently, this could be an indicative of a possible effect of **LSL60101** on OS balance.

From the structural chemical point of view, the nature of known I₂-IR ligands (Fig. 1) is relatively restricted and the pharmacophore moiety is generally related to 2-imidazoline-like structures.

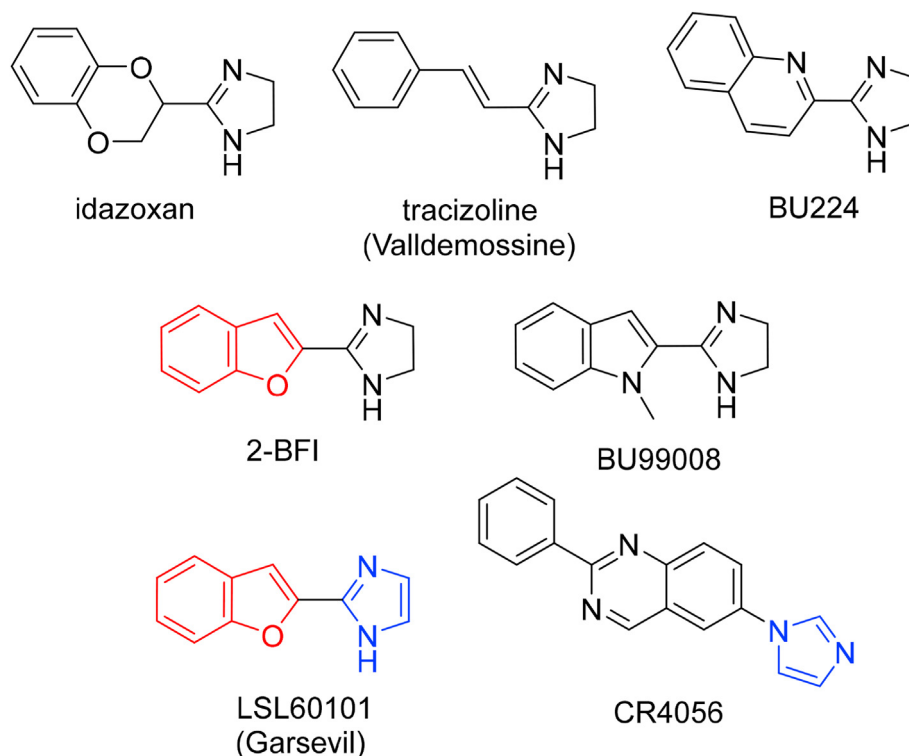


Fig. 1. Representative I₂-IR ligands.

Structural comparison of **LSL60101** with other known I₂-IR ligands, and in particular with 2-BFI that shares a benzofuran moiety, suggest a pharmacomodulation involving an unsaturation of the imidazole ring, a drug optimization strategy appealed in the design of new drugs. The presence of an imidazole ring in the successful CR4056 ligand encourages the proposal.

Herein we describe the synthesis and full characterization of ten benzofuranyl-2-imidazole derivatives to shed light on the structural-activity relationship of this family. Note, that the structural exploration involves substituents, either electron donating (methoxy) or electron attractor by inductive effect (bromide), located in different positions of the phenyl ring, and alkylation of the imidazole ring of the benzofuranyl-2-imidazole scaffold. We assessed the pharmacological profile of the ten analogues and selectivity through competition binding studies against the selective I₂-IR radioligand [³H]2-BFI. Selectivity versus two related targets, the imidoline I₁ receptor (I₁-IR) and the α₂-adrenergic receptor (α₂-AR) was evaluated through competition studies using the selective radioligands [³H]clonidine and [³H]RX821002 (2-methoxyidazoxan), respectively. Complementarily, we performed three-dimensional quantitative structure–activity relationship (3D-QSAR) studies of this compound family and predicted *in silico* the ADMET properties. **LSL60101** endowed with the best I₂-IR affinity and an excellent selectivity index regarding I₁-IR and α₂-AR was selected for further studies. We carried out preliminary drug metabolism and pharmacokinetics (DMPK) studies for **LSL60101**, including chemical stability, PAMPA-BBB permeability assay, solubility, cytotoxicity, microsomal stability, cytochromes inhibition, and safety. The hypothermic properties and FADD multifunctional protein (as a marker of neuroplasticity) regulation were also studied following several **LSL60101** treatments in mice. Pharmacokinetics was carried out prior to an *in vivo* treatment in a proper murine model of AD. Thus, we further assessed the neuroprotective effects of **LSL60101** by evaluating specific OS markers under oxidative damage and several transcription factors related to OS machinery in 5xFAD mice (an early-onset mouse transgenic model of AD).

2. Results and discussion

2.1. Chemistry

The preparation of the required final benzofuranyl-2-imidazoles was accomplished, based on previous described procedure [33], starting from the corresponding commercially available benzofuran-2-carboxylic acid derivatives (Scheme 1). Except for the commercially available benzofuran-2-carbonitrile, **2a**, the other derivatives **2b**, **2c**, and **2d**, were prepared in two steps. Treatment of the corresponding benzofuran-2-carboxylic acid derivatives with thionyl chloride and ammonium hydroxide furnished the carboxamides **1b**, **1c**, and **1d** in excellent yields. Dehydration reaction with phosphorus oxychloride gave benzofuran-2-carbonitriles, **2b**, **2c**, and **2d**, that were efficiently transformed in the corresponding benzofuran-2-carbimidates hydrochlorides **3a**, **3b**, **3c** and **3d** after treatment with ethereal HCl 2 M. To construct the imidazole moiety, the reaction with 2,2-dimethoxyethylamine was undertaken to give **4a**, **4b**, **4c** and **4d** in quantitative yields, that were treated with aqueous hydrochloric acid accomplish the attack of the nitrogen atom to the ketal electrophilic carbon, affording benzofuranyl-2-imidazoles **5a** (named **LSL60101**), **5b**, **5c** and **5d**. Recrystallization of **5a** as monocrystal confirmed its structure by X-ray crystallographic analysis (see supporting information S51).

To access hydroxybenzofuran-2-imidazole derivatives **6b** and **6c**, hydrolysis of the methylether group of **5b** and **5c** was achieved by treatment with hydrobromic acid. The alkylation of the N-imidazole of compound **5a** with methyl iodide gave compound **7a** and with ethyl iodide yielded **7aa**. Analogously, the reaction of **5b** and **5c** with ethyl bromide furnished the expected products **7b** and **7c** in excellent yields.

All final products **5a–5d**, **6b–6c** and **7a**, **7aa**, **7b** and **7c**, were completely characterized (see experimental section and supporting information S19–S29) and all the tested compounds possess a purity of at least 95% (see supporting information S30–S49).

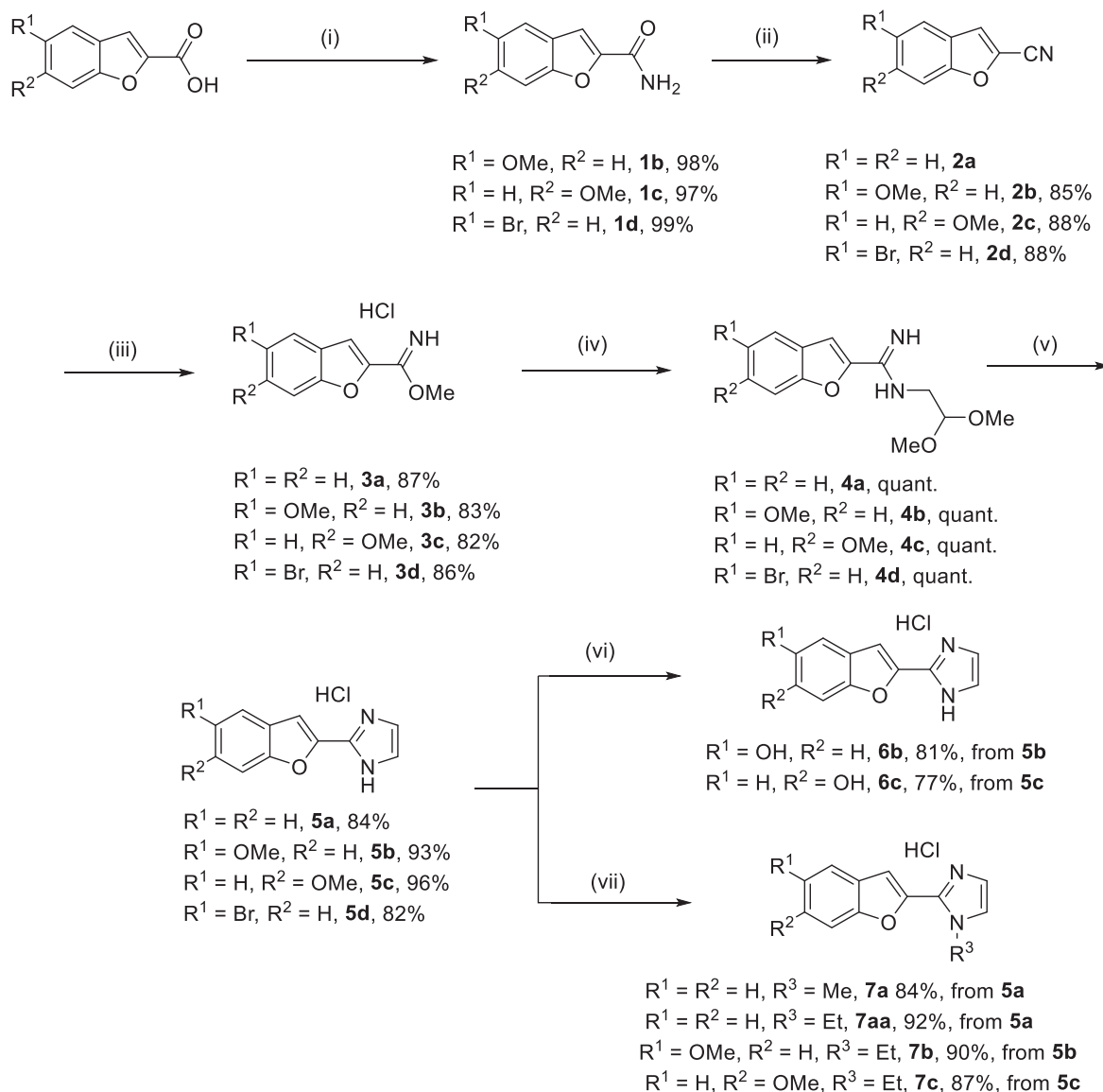
2.2. Pharmacological evaluation

2.2.1. Radioligand I₂-IR binding assays

The pharmacological profile of the ten compounds with the structures **5**, **6** and **7** (Scheme 1) was evaluated through competition binding studies against the selective I₂-IR radioligand [³H]2-BFI and the selective α₂-AR radioligand [³H]RX821002. The studies were performed in membranes from post-mortem human frontal cortex, a brain area that shows an important density of I₂-IR and α₂-AR. Idazoxan, a compound with well-established affinity for I₂-IR (pK_i = 7.41 ± 0.63) and α₂-AR (pK_i = 8.35 ± 0.16) was used as reference. The inhibition constant (K_i) for each compound was obtained and is expressed as the corresponding pK_i. The selectivity for these two receptors was expressed by the I₂/α₂ index, calculated as the antilogarithm of the ratio between pK_i values for I₂-IR and pK_i values for α₂-AR. Competition experiments against [³H]2-BFI were biphasic for most of the compounds (Table 1).

We have previously reported the affinity of 2-BFI in I₂-IR human brain (pK_{iH} = 9.08 and pK_{iL} = 7.15). The structural differences between 2-BFI and **LSL60101** rely on the presence of an additional double bond in the five membered ring, from a 2-imidazoline to an imidazole conferring a planar structure to **LSL60101** (see X-ray crystallography discussion in the experimental section). The mentioned structural difference rendered a decrease in the affinity to pK_{iH} = 8.17 ± 0.19 and pK_{iL} = 6.02 ± 0.10, with 34% occupancy of the high affinity site. The decreased affinity upon α₂-AR plays in our favor and selectivity had an excellent ratio of 3090.

Next, electron-donating groups in the phenyl ring, such as a methoxy group was considered. Thus, compounds **5b** and **5c** bearing a methoxy group in the position –5 and –6, gave affinity values of pK_i = 6.41 ± 0.16 and pK_{iH} = 6.77 ± 0.29 and pK_{iL} = 4.58 ± 0.39, respectively. The introduction of a 5-bromine furnished compound **5d** with similar affinity values as **LSL60101** (pK_{iH} = 8.63 ± 0.51 and pK_{iL} = 5.85 ± 0.18) but showing less selectivity against α₂-AR. The hydroxybenzofuran-2-imidazole derivatives **6b** and **6c** showed affinities of pK_{iH} = 9.57 ± 0.63 and pK_{iL} = 4.6 ± 0.26 and pK_i = 5.48 ± 0.11, respectively, with a drop in the I₂/α₂ selectivity in relation to their methoxy derivative partners **5b** and **5c**. Compounds **7a**, **7aa** and **7b** bearing a N-alkylated imidazole nucleus showed affinity that better fit to a two-site binding model with pK_{iH} = 6.99 ± 0.28 and pK_{iL} = 5.35 ± 0.21, pK_{iH} = 7.09 ± 0.42 and pK_{iL} = 4.72 ± 0.15, and pK_{iH} = 6.95 ± 0.16 and pK_{iL} = 4.16 ± 0.12, with high affinity site occupancy of 38, 22 and 35%, respectively. Compared to the non-alkylated partners **LSL60101** and **5b**, the additional N-alkyl group did not result in a significant increase in the pK_i value but in a drop in the I₂/α₂ selectivity. N-Ethyl substituted **7c** gave an outstanding pK_{iH} = 9.13 ± 0.47 value of I₂ affinity with a 12% high occupancy affinity site, whereas the non-alkylated homologous **5c** displayed a and pK_{iL} = 5.11 ± 0.06.



Scheme 1. Reagents and conditions: (i) SOCl_2 , toluene, 3 h, reflux; 25% aq. NH_4OH , rt; (ii) POCl_3 , dichloroethane, 75°C , 2 h; (iii) $\text{Et}_2\text{O}:\text{HCl}$ 2 M, 4°C , 48 h; (iv) 2,2-dimethoxyethylamine, methanol, 60°C , 16 h; (v) HCl 2 M, 60°C , 16 h; (vi) HBr 47%, 100°C , 7 h; (vii) NaH , methyl iodide or ethyl bromide, DMF, 0°C to rt, 75 min.

The study highlighted **LSL60101** as the most promising candidate of the benzofuran-2-imidazole family to tackle further *in vitro* and *in vivo* studies.

2.2.2. Comparison of I_2 -IR binding affinities of **LSL60101** across species

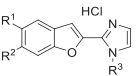
The literature is non-uniform in the I_2 -IR affinity values across species (human, rat, rabbit, mouse, and monkey), given the radioligand considered as a reference (idazoxan, 2-BFI) and the tissues used for analysis (from different anatomical parts: kidney, whole brain, cortex, etc). Thus, we made an effort in the comparison of affinities of standard I_2 -IR ligands, 2-BFI, trazolone, and clinically prominent [^{11}C]BU99008 and CR4056 [23]. When evaluating **LSL60101** a two-site model of binding was observed in human post-mortem brain cortical membranes with a $\text{pK}_{\text{IH}} = 8.17 \pm 0.19$ and $\text{pK}_{\text{IL}} = 6.02 \pm 0.10$, and an occupancy of the high site of 34%. In rat cerebral cortex using idazoxan as radioligand, **LSL60101** was reported a lower affinity than in human tissues, with a $\text{pK}_{\text{IH}} = 6.45$

and $\text{pK}_{\text{IL}} = 1.16$, but a higher percentage fraction of occupancy (79%) [34]. In mice brain cortical membranes, the competition curve against [^3H]2-BFI binding was significantly better with a two-site fit than a one-site binding model, providing a $\text{pK}_{\text{IH}} = 9.92 \pm 0.17$ and $\text{pK}_{\text{IL}} = 6.00 \pm 0.14$. These values were close to those found in human tissues including a similar occupancy of the high site (41%) supporting the *in vivo* experiments in mice.

2.3. 3D-QSAR study

The 3D-QSAR method was used to analyse the most significant descriptors that were interpreted in terms of identifying and quantifying structural elements important for I_2 -IR and α_2 -AR activity. The study was conducted on structurally diverse I_2 -IR ligands that were divided into two clusters, based on their chemical structures. Cluster 1 represents compounds synthesized in this manuscript, while cluster 2 contains bicyclic α -iminophosphonate I_2 -IR ligands previously described by our group (Fig. S1) [23]. To

Table 1
I₂-IR and α₂-AR Binding Affinities (pK_i) of compound idazoxan and 2-BFI and new compounds **5a-5d**, **6b**, **6c**, **7a**, **7aa**, **7b** and **7c**.

Compound R ¹ /R ² /R ³ General structure	^a [³ H]-2-BFI I ₂ pK _i one site	^b [³ H]-2-BFI I ₂ pK _i two sites		High-affinity site %	[³ H]-RX821002 α ₂ pK _i	Selectivity I ₂ /α ₂
	7.41 ± 0.63	7.87 ± 0.74	5.76 ± 0.57	40 ± 7	8.35 ± 0.16	—
2-BFI	8.31 ± 0.13	9.08 ± 0.22	7.15 ± 0.31	58 ± 9	4.58 ± 0.22	5370
5a, LSL60101 R ¹ = R ² = R ³ = H	6.67 ± 0.09	8.17 ± 0.19	6.02 ± 0.10	34 ± 4	3.18 ± 0.17	3090
5b R ¹ = OMe, R ² = R ³ = H	6.41 ± 0.16	—	—	—	3.94 ± 0.07	295
5c R ¹ = H, R ² = OMe, R ³ = H	5.88 ± 0.16	6.77 ± 0.29	4.58 ± 0.39	46 ± 9	3.01 ± 0.45	741
5d R ¹ = Br, R ² = H, R ³ = H	6.28 ± 0.18	8.63 ± 0.51	5.85 ± 0.18	20 ± 5	4.92 ± 0.25	23
6b R ¹ = OH, R ² = H, R ³ = H	4.87 ± 0.23	9.57 ± 0.63	4.6 ± 0.25	29 ± 5	3.84 ± 0.16	11
6c R ¹ = H, R ² = OH, R ³ = H	5.48 ± 0.11	—	—	—	3.76 ± 0.12	52
7a R ¹ = R ² = H, R ³ = Me	5.98 ± 0.08	6.99 ± 0.28	5.35 ± 0.21	38 ± 10	3.75 ± 0.12	170
7aa R ¹ = R ² = H, R ³ = Et	5.05 ± 0.10	7.09 ± 0.42	4.72 ± 0.15	22 ± 6	3.77 ± 0.08	19
7b R ¹ = OMe, R ² = H, R ³ = Et	4.96 ± 0.15	6.95 ± 0.16	4.16 ± 0.12	35 ± 3	4.21 ± 0.19	6
7c R ¹ = H, R ² = OMe, R ³ = Et	5.26 ± 0.08	9.13 ± 0.47	5.11 ± 0.06	12 ± 2	3.17 ± 0.25	123

^a Selectivity I₂-IR/α₂-AR expressed as the antilog (pK_i I₂-IR – pK_i α₂-AR).

^b The best fit of the data for most of the compounds was to a two-site binding model with high pK_i (pK_{iH}) and low pK_i (pK_{iL}) affinities for both binding sites, respectively.

compare and validate our results, we have added three I₂-IR standard ligands (tracizoline, idazoxan, and BU99008, Fig. 1), in both data sets. Structural diversity of prepared data set enabled us not only to deeper analyse the most important structural characteristics, but also to suggest modifications to come up with novel compounds with improved I₂-IR activity and selectivity.

The Pentacle program [38] was used for calculation of GRID independent descriptors (GRIND and GRIND2) and 3D-QSAR model building. The reliability and predictive power of the created 3D-QSAR models were assessed using different internal and external validation parameters (Tables S1 and S2). Obtained results indicated that both models possessed good predictive capability and could be used for activity prediction of newly designed compounds. PLS coefficient plots presented the most important variables with positive and negative influence on I₂-IR and α₂-AR activity (Figs. S2 and S3).

Compounds from cluster 1 are compounds reported here (Scheme 1) with pK_i ranges between 4.87 and 6.67 for I₂-IR, and 3.01–4.92 for α₂-AR, while cluster 2 compounds present our bicyclic α-iminophosphonate derivatives (Fig. S1) with pK_i ranging from 4.02 to 8.56 for I₂-IR, and 3.38–6.77 for α₂-AR. Comparing to molecules from cluster 2, cluster 1 compounds possess lower pK_i values for I₂-IR as well as α₂-AR.

The most potent compound from cluster 1, **LSL60101** (pK_i = 6.67), displayed all significant variables with the most positive impact on the activity. Positive influence on both I₂-IR and α₂-AR activity showed variables var24 (DRY-DRY: 9.60–10.00 Å) and var25 (DRY-DRY: 10.00–10.40 Å), respectively. They described the optimal distance range between two hydrophobic regions, around benzofuranyl and imidazole rings, which may be crucial for establishing favourable van der Waals interactions with amino acids in the active pocket of both receptors (Fig. 2a). Moreover, I₂-IR 3D-QSAR model pointed out var232 (DRY-O: 6.40–6.80 Å) as the variable with the strongest positive influence on I₂-IR binding

activity. This variable implies the importance of hydrogen bond donor group, –NH from imidazole ring, located at a certain distance from hydrophobic region, benzofuranyl ring (Fig. 2a). Contrary, it did not possess such a significant influence in the compounds from cluster 2, since they lack hydrogen bond donor groups (Fig. S4). GRIND variable O–N1 (var394: 6.40–6.80 Å) signified a positive influence of the imidazole ring on I₂-IR activity, describing the distance between hydrogen bond acceptor and donor probes located around nitrogen atoms (Fig. 2a). On the other hand, it did not show a significant effect on α₂-AR activity. Furthermore, the importance of hydrogen bonding interactions in the binding site of I₂ receptor was confirmed with variables var452 (O–TIP: 8.00–8.40 Å) and var503 (N1–TIP: 6.80–7.20 Å), which underlined optimal distances between the steric region around the benzofuranyl ring and –NH from the imidazole ring as a hydrogen bond donor or acceptor (Fig. 2a). Therefore, we can conclude that the substitution of the –NH imidazole group (R3) and losing of the hydrogen bond donating characteristics negatively correlated with I₂-IR binding activity and selectivity (**7a**, **7aa**, **7c**, **7b**). Analysis of α₂-AR 3D-QSAR model showed that the sole introduction of a hydrogen bond acceptor-group, at a certain distance from hydrophobic or steric region around heterocyclic ring, induced a positive impact on α₂-AR activity.

The compound with the lowest activity within the cluster 1 is **6b** (pK_i = 4.87). The introduction of a hydroxy or methoxy group on the carbon atom of the benzofuranyl nucleus resulted in reduced affinity, which could be described with var197 (TIP–TIP: 14.00–14.40 Å) and var350 (DRY–TIP: 10.40–10.80 Å) (Fig. 2b). Additionally, the unfavourable impact of these groups is also defined with the negative variable var408 (O–N1), which explains the distance of 12.00–12.40 Å between –NH of imidazole, as a hydrogen bond donor and the oxygen atom in hydroxy or methoxy substituent as a hydrogen bond acceptor (Fig. 2b). Based on these findings we can conclude that the introduction of a hydrogen bond

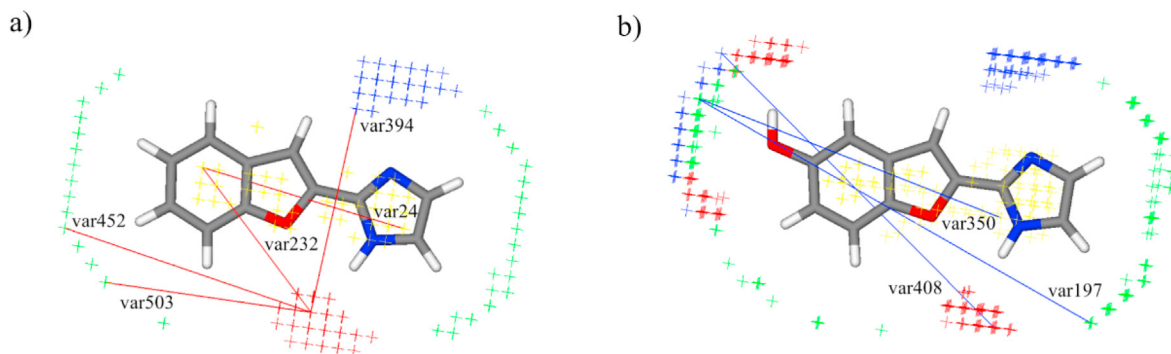


Fig. 2. Representation of positive interactions (in red) of **LSL60101** (a) and negative interactions (in blue) of **6b**; (b) in I_2 -IR 3D-QSAR model. The steric hot spots (TIP) are presented in green, hydrophobic regions (DRY) in yellow, H-bond acceptor regions (N1) in blue, and H-bond donor regions (N1) in red.

acceptor substituent on the benzofuranyl ring may not be considered as the most complementary with the binding site of I_2 -IR.

2.4. *In silico* ADMET analysis of physicochemical and pharmacokinetic parameters

The drug discovery pipeline has more and more relied on *in silico* predictions to optimize lead compounds and reduce investments [39]. *In silico* ADMET prediction aims to evaluate individual ADMET behaviours of examined compounds. Pharmacokinetic properties such as absorption, distribution, metabolism, excretion, and toxicity (ADMET) profiling of compounds were determined using ADMET Predictor software [40], while physico-chemical parameters were assessed with SwissADME online programme [41]. The obtained results are presented in Tables S3 and S4. Based on the results obtained from the performed calculations, we can conclude that all studied compounds present good water solubility and lipophilicity. Compounds reported here satisfy the Lipinski's Rule of 5, which supports their drug-likeness properties and potential chance to be orally bioavailable. Moreover, the polarity of compounds was evaluated by the TPSA (topological polar surface area) descriptor and results revealed that benzofuranyl-2-imidazoles possessed lower polarity, similar to idazoxan, when compared to previously described bicyclic α -iminophosphonate derivatives (see supporting information, Fig. S1) [23]. Regarding pharmacokinetic properties, we noted that all molecules possessed high BBB permeation. Compared to standard molecules, such as idazoxan, all examined compounds possessed lower percentage of unbound drug in plasma. Furthermore, this family showed lower metabolic CYP risk and TOX risk comparing to idazoxan and bicyclic α -iminophosphonate derivatives. P-gp is believed to play an important role in drug distribution and resistance to CNS drug treatment. The examined compounds were not identified as potential substrates for P-gp transporters. Since blocking hERG channels represents a major therapeutic challenge in drug discovery, we note that the compounds synthesized in this manuscript did not show affinity to inhibit hERG channels.

The absence of warnings of this theoretical study gave us confidence for undertaking further *in vitro* and eventually, *in vivo* experiments to assess the benzofuranyl-2-imidazole family and **LSL60101** as a neuroprotective agent.

2.5. Blood brain barrier permeation assay

Considering the localization of I_2 -IR in the CNS, a good ability to cross the BBB is an essential requirement for developing effective

I_2 -IR ligands with potential therapeutic applications in the neuroprotective field. Guaranteed by the *in silico* parameters the *in vitro* permeability (P_e) of all the novel compounds was determined by using the PAMPA-BBB permeability assay (Table 2). The new compounds prepared were well above the threshold established for high BBB permeation ($P_e > 5.198 \times 10^{-6} \text{ cm s}^{-1}$), except for compounds **6b** and **6c**. The aforementioned two compounds bear a hydroxyl group increasing their polarity and decreasing their capability to permeate the artificial PAMPA-BBB membrane with P_e values of $0.1 \pm 0.03 \times 10^{-6} \text{ cm s}^{-1}$ and $0.32 \pm 0.1 \times 10^{-6} \text{ cm s}^{-1}$, respectively. In particular, the most I_2 -IR affine compound **LSL60101** had a P_e value of $13.6 \pm 0.4 \times 10^{-6} \text{ cm s}^{-1}$ and was considered suitable to envisage further *in vitro* and *in vivo* studies oriented to in-depth the pharmacological profile of the new family of I_2 -IR ligands.

According to these data, compounds including a hydroxyl group in its structure, such as **6b** and **6c**, were not suitable for considering their potential in neurodegenerative diseases. In particular, **LSL60101** showed the best affinity and selectivity values and since it had a good ability to cross the BBB it will be used to undertake further studies.

2.6. Selectivity I_2 -IR versus I_1 -IR in **LSL60101**

LSL60101 showed a remarkable affinity for I_2 -IR and selectivity I_2/α_2 -AR with a ratio 3090. Then, we assessed the affinity/selectivity

Table 2
Permeability results ($P_e \text{ } 10^{-6} \text{ cm s}^{-1}$) from the PAMPA-BBB assay for new report compounds and their prediction of BBB permeation.

Compound	^a $P_e \text{ } 10^{-6} \text{ cm s}^{-1}$	^b Prediction
Idazoxan	3.3 ± 0.1	CNS \pm
2-BFI	6.1 ± 0.2	CNS+
5a, LSL60101	13.6 ± 0.4	CNS+
5b	8.3 ± 1.2	CNS+
5c	7.6 ± 0.1	CNS+
5d	20.3 ± 0.2	CNS+
6b	0.32 ± 0.1	CNS-
6c	0.1 ± 0.03	CNS-
7a	17.4 ± 0.85	CNS+
7aa	19.2 ± 1.1	CNS+
7b	12.4 ± 0.8	CNS+
7c	14.85 ± 0.1	CNS+

^a PBS/EtOH (70:30) was used as solvent. Values are expressed as mean \pm SD of at least three independent experiments.

^b The *in vitro* permeability (P_e) of fourteen commercial drugs through lipid extract of porcine brain membrane together with the test compounds were determined (for the commercial drug values see Table S5).

for the very close receptors I₁-IR. Specific binding of [³H]clonidine (20 nM) to I₁-IR of rat or human hypothalamic membranes was accomplished after pre-incubation with benextramine (10 μM) to alkylate population of α₂-AR. Under these experimental conditions [³H]clonidine only labelled I₁-IR and in drug competition experiments moxonidine, a known I₁-IR selective compound, showed subnanomolar affinity for these I₁-sites; K_{iH} = 0.2 nM; K_{iL} = 12 μM. **LSL60101** displayed a very low affinity for I₁-IR, in rat samples K_i = 115 μM and in human samples K_i = 250 μM.

2.7. Acute toxicity

Based on the excellent affinity/selectivity upon I₂-IR of **LSL60101**, the safety evaluation was undertaken to determine the acute toxicity of the compound. **LSL60101** was safe up to a dose level of 100 mg/kg body weight after an intraperitoneal administration, since the LD₅₀ was considered to be greater than 100 mg/kg (Probit analysis) in male albino mice (lack of toxicity in the range of doses tested: 10–100 mg/kg; n = 10 mice per dose tested).

2.8. ADME-DMPK profiling of **LSL60101**

With a compound showing promising binding properties/selectivity, devoid to α₂-AR and I₁-IR, and optimal safety, we undertook *in vitro* assays to define its physicochemical properties and chemical stability.

The solubility of **LSL60101** in 1% DMSO and 99% PBS buffer was excellent (52.5 μM). For a better definition, the solubility of **LSL60101** at different pH 1.13, 4.61 and 6.97, simulating the pH range of the gastric and intestinal fluids, was studied (see supporting information S10). Following the solubility terms established in *European Pharmacopoeia* vs.10.0, **LSL60101** is a soluble substance at pH 1.13 and 4.61 and a very slightly soluble substance at pH 6.97 (Table S6).

The chemical evaluation of **LSL60101** implied forced degradation studies under different stress conditions for a period of nine weeks, monitoring weekly the assays by HPLC and ¹H NMR. In particular, **LSL60101** was subjected to the effect of daylight with temperatures between 0 and 23 °C and a relative humidity of 25–85%, to the effect of high temperature (thermal stability at 75 °C), and to the continuous light of a 100W (230V) bulb. Analysis by HPLC showed that the compound was completely stable under all the aforementioned conditions. Calculated lipophilicity of **LSL60101** referring to the consensus log P_{o/w} value calculated using the SwissADME program for five predictive log P_{o/w} models, iLOGP, XLOGP3, WLOGP, MLOGP and SILICOS-IT, which gave values of 1.51, 2.16, 2.82, 1.15 and 3.02, respectively. Therefore, the calculated log P_{o/w} and the other parameters of Lipinski were within the limits and the compounds are suitable for undertaking the characterization of *in vitro* ADME properties.

Microsomal stability, which is widely used to determine the likely degree of primary metabolic clearance in the liver, was assessed in human and mouse recombinant microsomes. The data shown in Table S7 reveals a 36% percentage of remaining compound, after 60 min of incubation in mouse microsomes, and 58% in human, indicating moderate differences in the metabolism depending on the species. The t_{1/2} is 1.4-fold bigger in human than in mice, therefore the difference should be taken into consideration through additional preclinical studies.

The inhibition potential of **LSL60101** was evaluated using recombinant human cytochrome P450 enzymes [CYP1A2, CYP2C9, CYP2C19, CYP2D6, CYP3A4 (7-BFC) and CYP3A4 (DBF)] and probe substances with fluorescent detection. The results depicted in Table S8 showed no inhibition of the cytochromes considered at 10 μM concentration. Taking into account the range of nM in the

affinity values of **LSL60101** it is not expected that at therapeutic doses the compound may interfere with the cytochrome P450-mediated metabolism of other drugs.

The plasma stability of **LSL60101** assessed in humans pooled from healthy donors was measured up to 6 h (0 h, 1 h, 2 h and 6 h) revealing 100, 83, 77 and 57% of the remaining percentage (Table S9). In mouse plasma **LSL60101** was inert under the conditions studied, remaining as 100% of the initial compound after 6 h (Table S10).

The extent of plasma protein binding was slightly superior in human than in mouse plasma. The fraction unbound value is also reported in Table S11. Whereas a 7.1% of **LSL60101** can be found in humans as free drug, a 16.0% was observed in mouse.

The effect of **LSL60101** over the activity of hERG, an important safety issue in drug discovery, was assessed and showed an inhibitory activity (%) of 4 ± 1 at 10 μM concentration, discarding any worries on this issue.

2.9. Cytotoxicity

In order to exclude compounds with adverse cellular effects, the newly synthesized compounds were evaluated for cytotoxicity. Human primary cells are physiologically more relevant. However, because of the difficulties of working with primary cultures, immortalized cell lines were used as an *in vitro* screening tool for cytotoxicity. In a panel of cancer cell lines, including LN-229 (glioblastoma), Capan-1 (pancreatic adenocarcinoma), HCT-116 (colorectal carcinoma), NCI-H460 (lung carcinoma), DND-41 (acute lymphoblastic leukemia), HL-60 (acute myeloid leukemia), K-562 (chronic myeloid leukemia) and Z-138 (non-Hodgkin lymphoma) cell lines, none of the compounds displayed any cytotoxicity at 100 μM (the highest concentration tested), as determined by a real-time IncuCyte proliferation assay.

2.10. Pharmacokinetics

The pharmacokinetic profile of **LSL60101** was investigated prior to the treatment of a murine model of AD (5xFAD). Following a single oral administration of 10 mg/kg of **LSL60101** in CD1 mice, plasma concentrations of drug were found after 15 min of treatment and were detected for 24 h. Absorption of drug from the gastrointestinal tract was slowly reaching C_{max} (3.24 μM) at 2 h after dosing and t_{1/2β} was around 7 h. The narrow differences in AUC₀[∞] and AUC₀⁸ showed complete exposure, good bioavailability and appropriate elimination of **LSL60101** to reach the therapeutic potential of I₂-IR ligands in the experimental conditions described (Fig. 3).

Furthermore, the remarkable affinity of **LSL60101** for I₂-IR (pK_i in mouse brain cortical membranes ranged from 9.92 to 6) and the excellent selectivity ratio I₂/α₂-AR (3090) could guarantee, from the kinetic profile observed in plasma, that the concentrations reached at the site of action are enough to demonstrate the efficacy of this drug.

Overall, these studies confirmed that **LSL60101** is orally bioavailable and metabolically stable and can be used for further *in vivo* experiments.

2.11. Hypothermic effects of **LSL60101** in naïve mice

Several previous studies have proven the induction of acute hypothermia by I₂-IR ligands in rats [42,43] and mice [21–23]. In this regard, the present study evaluated the hypothermic effects of **LSL60101** in a wide range of doses (1, 5, 10, 20, 30, 50 mg/kg i.p.) in adult male and female CD1 mice at different times post-injection. The results showed a sharp drop in core body temperature

Pharmacokinetic parameters	
AUC _{0-∞} (ug*h/ml)	2.6
AUC _{0-t} (ug*h/ml)	2.7
T _{max}	2 h
C _{max}	0.6 µg/ml
t _{1/2 β}	6.7 h

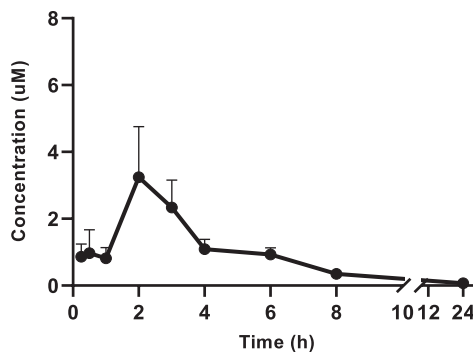


Fig. 3. Plasma concentration of **LSL60101** at different times (15 min–24 h) after an oral administration of 10 mg/kg, determined by HPLC/UV-VS at 290 nm. Basic pharmacokinetic parameters were calculated.

(ranging from -1.1 to -3.9 °C) for the larger dose tested (50 mg/kg) and observed 1 and up to 2 h post-injection (Fig. 4). Core body temperature returned to basal levels 3 h after drug administration.

The present results, in line with prior data [42], suggest the need for high doses of **LSL60101** to induce the expected hypothermia characteristic of I₂-IR ligands [21–23,43]. As for the role of this acute pharmacological effect, hypothermia is known to provide neuroprotection in models of cerebral ischemia; even mild temperature drops can cause significant neuroprotection [44]. In fact, hypothermia has been used to improve the neurological outcome under various pathological conditions, including stroke and traumatic brain injury [45,46]. In this line of thought, **LSL60101** has proven to partially prevent neuronal death in rats following neonatal axotomy [36], and thus, its hypothermic effects might be a relevant feature that could be mediating certain degree of neuroprotection.

Although the agonist or antagonist nature of I₂-IR ligands has been a topic of debate [2], it has been suggested that I₂-IR agonists reliably decrease body temperature in a highly quantitative manner in rodents [42], suggesting this assay could be used as a sensitive *in vivo* assay for studying I₂ receptor ligands, and in line with the hypothermic effects observed in the present study in mice treated with **LSL60101**.

2.12. Effects of acute **LSL60101** on hippocampal FADD protein content in naïve mice

In the context of neuroprotection, FADD adaptor emerges as a key multifunctional protein involved in the mechanisms

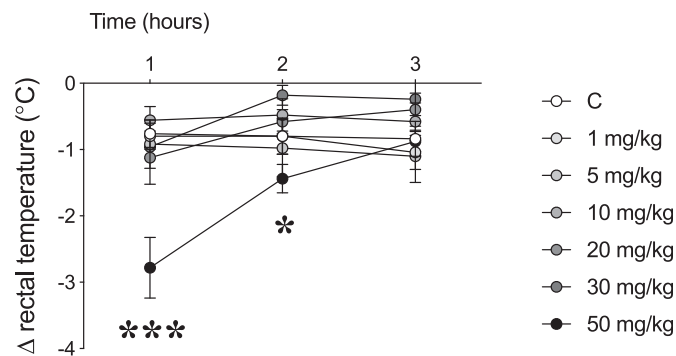


Fig. 4. Acute effects of **LSL60101** treatment on core body temperature in mice. Symbols represent means \pm SEM of the difference (Δ , 1, 2 or 3 h minus basal value) in body temperature (°C) for each treatment group. *** $p < 0.001$ and * $p < 0.05$ when comparing the dose of 50 mg/kg with the control group (repeated measures ANOVA followed by Sidak's comparison test).

controlling cell fate regulation, balancing pro-apoptotic and/or neuroprotective actions in rodents [21,47,48]. The acute treatment with a high dose of **LSL60101** (50 mg/kg, i.p.) significantly decreased (by $\sim 34\%$) hippocampal FADD protein content as compared to vehicle-treated mice (Fig. 5). The present results replicated earlier studies in which other I₂-IR ligands decreased FADD hippocampal content [21,23], and suggested the induction of non-apoptotic (e.g., neuroplastic and/or neuroprotective) actions initiated by acute **LSL60101** treatment in mice brain and in parallel to the hypothermic effects.

2.13. Effects of chronic **LSL60101** at a low dose in a mice model of Alzheimer's disease

Accumulating evidence support that I₂-IR exert neuroprotective roles in a plethora of neurodegenerative disorders, such as AD [8,9,11,49,50]. Previous studies suggested that I₂-IR in the CNS are mainly located on the outer membrane of mitochondria in astrocytes [51]. Given that alterations in mitochondrial function promote an increased ROS production, which combined with an altered antioxidant defence contribute to the early stages of AD before the development of A β pathology and cognitive dysfunction [29,30,52], here we tested the effects of a low dose of **LSL60101** administered following a chronic paradigm (1 mg/kg/day, for 4 weeks) on specific OS markers under oxidative damage in 5XFAD mice, an early-onset mouse transgenic model of AD, and as compared to a wild type strain. The results showed increased gene expression of the so-called antioxidant response element (AREs), such as heme oxygenase 1 (Hmox1), aldehyde dehydrogenase 2 (Aldh2) and iNOS [53] in 5xFAD vs. wild type mice (Fig. 6). By contrast, in 5xFAD mice treated with **LSL60101**, the expression of those decreased in a significant way.

On the other hand, an excess in ROS is removed by antioxidant enzymes (e.g., superoxide dismutase, SOD1, and glutathione peroxidase, GPX-1). 5XFAD mice showed a significant decrease in both proteins levels in reference to wild type mice. Interestingly, **LSL60101** was able to significantly increase the levels of these key protein, indicating that **LSL60101** induced the activation of a cellular signalling cascade that led to a reduced OS, and that in turn could have a neuroprotective role in an oxidative environment related with neurodegenerative processes such as AD (Fig. 7).

These results are in agreement with recent studies that demonstrated a key role for I₂-IR ligands in the OS process. In particular, 2-BFI (a selective ligand to I₂-IR), decreased OS and altered the level of anti-oxidant enzymes in an AD rat model [54], protecting against OS-induced astrocytic cell death [55]. Ultimately, previous work from our group reported a decrease in hydrogen peroxide levels and OS markers induced by the I₂-IR ligands **MCR5**

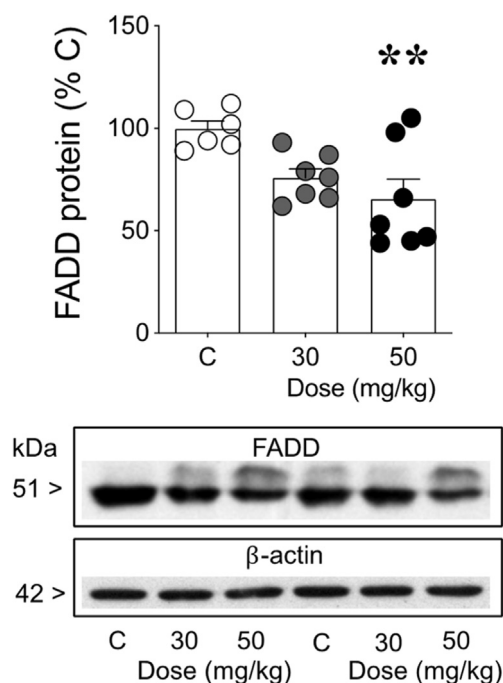


Fig. 5. Acute effects of **LSL60101** (30 or 50 mg/kg, i.p.) on hippocampal FADD protein. Columns are means \pm SEM of FADD content (% C) for each treatment group. Individual symbols are shown for each animal. One-way ANOVA followed by Sidak's multiple comparisons tests: $**p < 0.01$ vs. C (control-treated mice). Representative immunoblots depicting the labelling of FADD and β -actin (as a loading control) for each treatment group are shown below.

and **MCR9** in aged SAMP8 mice [22]. Recently, we demonstrated that **LSL60101** can ameliorate the AD hallmarks and neuroinflammation [56]. Moreover, the chronic treatment with **LSL60101** led to the induction of reactive astrocytes and the up-regulation of the expression of the astrocyte marker glial fibrillary acidic protein (GFAP) [34]. As mentioned, astrocytes are the main supportive cells in the CNS and are significantly involved in the redox homeostasis [57], and thus, and as a consequence, this could be proposed as a possible effect of **LSL60101** on OS balance.

3. Conclusions

We have evaluated the binding and selective properties upon I_2 -IR in human brain tissues of a series of benzofuranyl-2-imidazoles diversely substituted in both benzofuranyl and imidazole rings. Due to the lack of structural description of these receptors, 3D-QSAR and *in silico* physicochemical properties were performed in order to determine the relevant elements that may allow the further structural optimization of new molecules. The secure theoretical DMPK of the family led us to undertake *in vitro* studies including PAMPA to confirm their penetration into the CNS to address neurodegenerative issues. The safe *in vitro* DMPK and cytotoxicity assays of the selected **LSL60101** opened the door to *in vivo* studies. After the determination of its pharmacokinetic profile, the treatment of animals with **LSL60101** confirmed a decrease in the content of hippocampal FADD protein, a key signalling mediator of neuroprotective actions. The I_2 -IR ligand **LSL60101** also fostered a diminution in oxidative stress biomarkers in an AD murine model (5xFAD). Thus, the modulation of I_2 -IR by **LSL60101** is proposed as a promising opportunity for addressing AD therapeutics and invites for the further design of new promising benzofuranyl-2-imidazole-base structures to be added to the scarce arsenal of I_2 -IR ligands.

4. Experimental section

4.1. Chemistry

Reagents, solvents and starting products were acquired from commercial sources. The term "concentration" refers to the vacuum evaporation using a Büchi rotavapor. When indicated, the reaction products were purified by "flash" chromatography on silica gel (35–70 μ m) with the indicated solvent system. IR spectra were performed in a Spectrum Two FT-IR Spectrometer, and only noteworthy IR absorptions (cm^{-1}) are listed. NMR spectra were recorded in $\text{DMSO-}d_6$ at 400 MHz (^1H) and 100.6 MHz (^{13}C), and chemical shifts are reported in δ values downfield from TMS or relative to residual $\text{DMSO-}d_6$ (2.50 ppm, 39.5 ppm) as an internal standard. Data are reported in the following manner: chemical shift, multiplicity, coupling constant (J) in hertz (Hz) and integrated intensity. Multiplicities are reported using the following abbreviations: s, singlet; d, doublet; dd, double doublet; q, quadruplet; t, triplet; m, multiplet; br s, broad signal. The accurate mass analyses were carried out using a LC/MSD-TOF spectrophotometer. HPLC-MS (Agilent 1260 Infinity II) analysis was conducted on a Poroshell 120 EC-C15 (4.6 mm \times 50 mm, 2.7 μ m) at 40 $^\circ\text{C}$ with mobile phase A ($\text{H}_2\text{O} + 0.05\%$ formic acid) and B (ACN + 0.05% formic acid) using a gradient elution and flow rate 0.6 mL/min. The DAD detector was set at 254 nm, the injection volume was 5 μL , and oven temperature was 40 $^\circ\text{C}$. All tested compounds possess a purity of at least 95%.

4.1.1. General procedures for the synthesis of benzofuran-2-carboxamides **1b**, **1c** and **1d**

Thionyl chloride (1.65 equiv) was added to a suspension of benzofuran-2-carboxylic acid derivatives (1 equiv) in anhydrous toluene (0.4 mmol/mL). After stirring the mixture for 3 h, at reflux, the reaction was cooled and concentrated. Then, the resulting benzofuran-2-carbonyl chloride derivative (1 equiv) was added in small portions to an ice-cold solution of 25% aq. NH_4OH (0.5 mmol/mL). Upon completion of the addition the reaction mixture was allowed to reach rt and a precipitate was formed. The solid was collected by filtration, washed with cold water and dried under vacuum.

4.1.1.1. 5-Methoxybenzofuran-2-carboxamide (1b). Following the general procedure, thionyl chloride (17.2 mmol, 1.25 mL), 5-bromobenzofuran-2-carboxylic acid (10.4 mmol, 2.0 g), anhydrous toluene (25 mL) and 25% aq. NH_4OH (20 mL) gave **1b** (1.87 g, 98%) as a beige solid.

4.1.1.2. 6-Methoxybenzofuran-2-carboxamide (1c). Following the general procedure, thionyl chloride (8.60 mmol, 0.63 mL), 6-methoxybenzofuran-2-carboxylic acid (5.20 mmol, 1.0 g), anhydrous toluene (13 mL) and 25% aq. NH_4OH (10 mL) gave **1c** (930 mg, 97%) as a beige solid.

4.1.1.3. 5-Bromobenzofuran-2-carboxamide (1d). Following the general procedure, thionyl chloride (13.7 mmol, 1.0 mL), 5-bromobenzofuran-2-carboxylic acid (8.30 mmol, 2.0 g), anhydrous toluene (21 mL) and 25% aq. NH_4OH (17 mL) gave **1d** (1.98 g, 99%) as a white solid.

4.1.2. General procedure for the synthesis of benzofuran-2-carbonitrile **2b**, **2c** and **2d**

Phosphoryl chloride (3 equiv) was added to a solution of benzofuran-2-carboxamide derivative (1 equiv) in dichloroethane (0.48 mmol/mL). The reaction was stirred at 75 $^\circ\text{C}$ for 2 h. Then, the reaction mixture was evaporated and neutralized with saturated NaHCO_3 solution. The aqueous phase was extracted with AcOEt , the

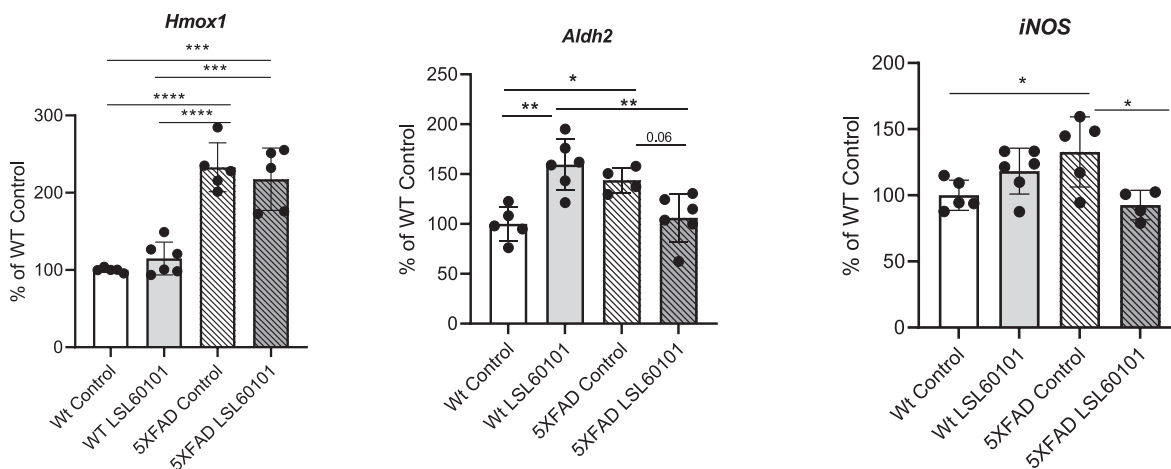


Fig. 6. Chronic effects of **LSL60101** (1 mg/kg/day, per os.) on *Hmox1*, *Aldh2* and *iNOS* gene expression in hippocampus. Columns are the mean \pm SEM for each treatment group. Individual symbols are shown for each animal. Means were compared with two-way ANOVAs, followed by Tukey-Kramer multiple comparison post-hoc analysis: **** p < 0.0001; *** p < 0.001; ** p < 0.01; * p < 0.05 vs. Wt Controls.

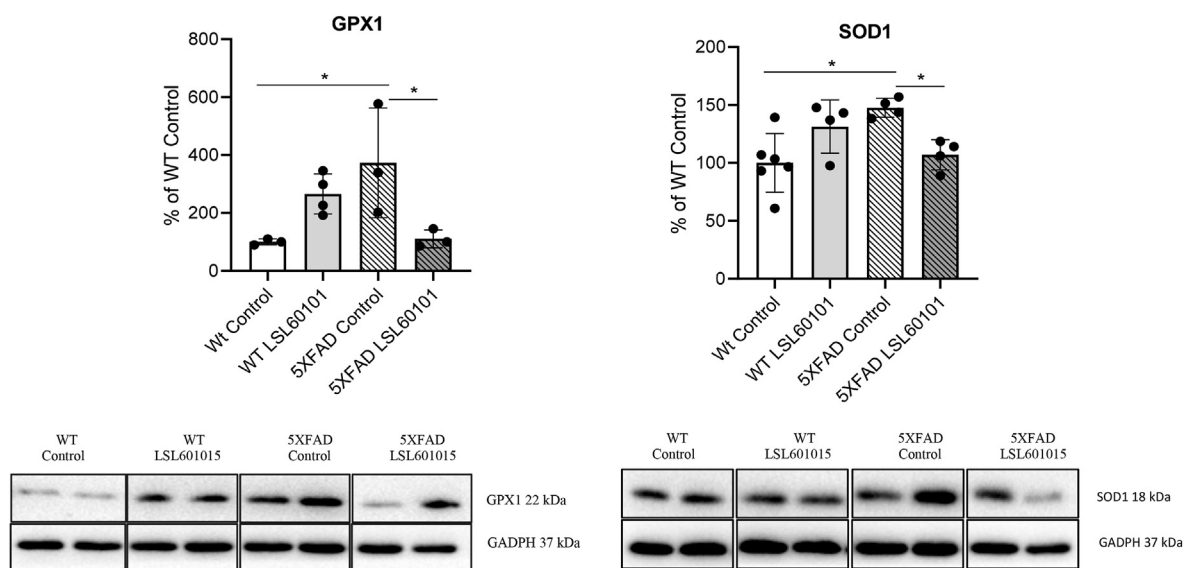


Fig. 7. Chronic effects of **LSL60101** (1 mg/kg/day, per os.) on the expression of SOD1 and GPX-1 protein levels in hippocampus. Columns are the mean \pm SEM for each treatment group. Individual symbols are shown for each animal. Means were compared with two-way ANOVAs, followed by Tukey-Kramer multiple comparisons post-hoc analysis. * p < 0.01 vs. Wt control mice).

combined organic phases were washed with brine, dried over Na_2SO_4 , and evaporated to give a residue, which was purified by flash column chromatography.

4.1.2.1. 5-Methoxybenzofuran-2-carbonitrile (2b). Following the general procedure, **1b** (9.62 mmol, 1.84 g), dichloroethane (20 mL) and phosphoryl chloride (28.9 mmol, 2.70 mL) gave **2b** (1.42 g, 85%) as a beige solid, after column chromatography (dichloromethane 100%).

4.1.2.2. 6-Methoxybenzofuran-2-carbonitrile (2c). Following the general procedure, **1c** (4.87 mmol, 930 mg), dichloroethane (10 mL) and phosphoryl chloride (14.6 mmol, 1.36 mL) gave **2c** (740 mg, 88%) as a beige solid, after column chromatography (dichloromethane 100%).

4.1.2.3. 5-Bromobenzofuran-2-carbonitrile (2d). Following the general procedure, **1d** (7.92 mmol, 1.90 g), dichloroethane (17 mL) and

phosphoryl chloride (23.8 mmol, 2.21 mL) gave **2d** (1.55 g, 88%) as a white solid, after column chromatography (dichloromethane 100%).

4.1.3. General procedure for the synthesis of methyl benzofuran-2-carbimidate hydrochlorides **3a**, **3b**, **3c** and **3d**

The 2-cyanobenzofuran derivative (1 equiv) was dissolved in ethereal HCl 2 M (0.25 mmol/mL) and methanol (5 mmol/mL). The resulting mixture was kept at 4 °C for 48 h. The resulting solid was filtered, washed with cold ether and dried in order to obtain the desired carbimidate hydrochloride.

4.1.3.1. Methyl benzofuran-2-carbimidate hydrochloride (3a). Following the general procedure, benzofuran-2-carbonitrile (6.99 mmol, 1.0 g), ethereal HCl 2 M (28 mL) and methanol (1.4 mL) gave **3a** (1.29 g, 87%) as a white solid.

4.1.3.2. *Methyl 5-methoxybenzofuran-2-carbimidate hydrochloride (3b)*. Following the general procedure, **2b** (8.08 mmol, 1.40 g), ethereal HCl 2 M (32 mL), methanol (2 mL) gave **3b** (1.62 g, 83%) as a white solid.

4.1.3.3. *Methyl 6-methoxybenzofuran-2-carbimidate hydrochloride (3c)*. Following the general procedure, **2c** (4.04 mmol, 700 mg), ethereal HCl 2 M (16 mL) and methanol (1 mL) gave **3c** (797 mg, 82%) as a white solid.

4.1.3.4. *Methyl 5-bromobenzofuran-2-carbimidate hydrochloride (3d)*. Following the general procedure, **2d** (4.82 mmol, 1.10 g), ethereal HCl 2 M (19 mL) and methanol (1 mL) gave **3d** (1.20 g, 86%) as a white solid.

4.1.4. General procedure for the synthesis of *N*-(2,2-dimethoxyethyl)benzofuran-2-carboximidamide **4a**, **4b**, **4c** and **4d**

A solution of 2,2-dimethoxyethylamine (1.1 equiv) and methyl benzofuran-2-carbimidate hydrochloride derivative (1 equiv) in methanol (0.47 mmol/mL) was stirred at 60 °C for 16 h. The mixture was evaporated to dryness, which was used directly in the next step without further purification.

4.1.4.1. *N*-(2,2-dimethoxyethyl)benzofuran-2-carboximidamide (**4a**). Following the general procedure, **3a** (5.20 mmol, 1.10 g), 2,2-dimethoxyethylamine (5.72 mmol, 0.62 mL) and methanol (11 mL) gave **4a** (1.29 g, quantitative) as a beige solid.

4.1.4.2. *N*-(2,2-Dimethoxyethyl)-5-methoxybenzofuran-2-carboximidamide (**4b**). Following the general procedure, **3b** (4.34 mmol, 1.05 g), 2,2-dimethoxyethylamine (4.78 mmol, 0.52 mL) and methanol (9 mL) gave **4b** (1.29 g, quantitative) as a beige solid.

4.1.4.3. *N*-(2,2-Dimethoxyethyl)-6-methoxybenzofuran-2-carboximidamide (**4c**). Following the general procedure, **3c** (2.93 mmol, 708 mg), 2,2-dimethoxyethylamine (3.22 mmol, 0.35 mL) and methanol (6 mL) gave **4c** (815 mg, quantitative) as a beige solid.

4.1.4.4. *N*-(2,2-Dimethoxyethyl)-5-bromobenzofuran-2-carboximidamide (**4d**). Following the general procedure, **3d** (2.01 mmol, 584 mg), 2,2-dimethoxyethylamine (2.21 mmol, 0.24 mL) and methanol (4 mL) gave **4d** (657 mg, quantitative) as a beige solid.

4.1.5. General procedure for the synthesis of 2-(benzofuran-2-yl)-1H-imidazole hydrochlorides **LSL60101**, **5b**, **5c** and **5d**

The corresponding *N*-(2,2-dimethoxyethyl)benzofuran-2-carboximidamide was treated with HCl 2 M (0.1 mmol/mL) and the resulting mixture was stirred at 60 °C for 16 h. After cooling, the solution was washed with dichloromethane. The aqueous layer was basified with NaOH 5 M and the free base extracted with AcOEt. The combined organic phases were washed with brine, dried over Na₂SO₄, and evaporated to give a residue which was dissolved in diethyl ether/ethanol (5:1). Ethereal HCl 2 M (1.5 mmol/mL) was added and the precipitated salt was collected by filtration and was crystallized with acetonitrile.

4.1.5.1. 2-(Benzofuran-2-yl)-1H-imidazole hydrochloride (**5a**). Following the general procedure, **4a** (5.20 mmol, 1.29 g), HCl 2 M (52 mL) and ethereal HCl 2 M (3.5 mL) gave **LSL60101** (960 mg, 84%) as a white solid. IR (ATR) 3477, 3168, 2535, 1651, 1457, 1310, 1140, 1009, 879, 737, 706 cm⁻¹. ¹H NMR (400 MHz, DMSO-*d*₆) δ 7.40 (t, *J* = 7.5 Hz, 1H), 7.52 (t, *J* = 8.5 Hz, 1H), 7.74 (d, *J* = 8.5 Hz, 1H), 7.83 (s,

2H), 7.88 (d, *J* = 7.5 Hz, 1H), 8.12 (s, 1H). ¹³C NMR (100.6 MHz) δ 109.8, 111.6, 120.8 (2C), 122.9, 124.4, 127.1, 127.3, 135.1, 140.6, 154.6. HRMS C₁₁H₉N₂O [M+H]⁺ 185.0709; found, 185.0706. Purity 99.6% (t_R = 3.08 min).

4.1.5.2. 2-(5-Methoxybenzofuran-2-yl)-1H-imidazole hydrochloride (**5b**). Following the general procedure, **4b** (4.10 mmol, 1.14 g), HCl 2 M (41 mL) and ethereal HCl 2 M (2.7 mL) gave **5b** (950 mg, 93%) as a white solid. IR (ATR) 3449, 3076, 2587, 1647, 1457, 1434, 1206, 1157, 1018, 812, 776, 712 cm⁻¹. ¹H NMR (400 MHz, DMSO-*d*₆) δ 3.81 (s, 3H), 7.08 (dd, *J* = 9.0, 2.5 Hz, 1H), 7.38 (d, *J* = 2.5 Hz, 1H), 7.61 (d, *J* = 9.0 Hz, 1H), 7.82 (s, 2H), 8.10 (s, 1H). ¹³C NMR (100.6 MHz) δ 55.7, 104.4, 110.2, 112.2, 116.5, 120.7 (2C), 127.8, 135.0, 141.1, 149.5, 156.5. HRMS C₁₂H₁₁N₂O₂ [M+H]⁺ 215.0815; found, 215.0816. Purity 98.5% (t_R = 3.19 min).

4.1.5.3. 2-(6-Methoxybenzofuran-2-yl)-1H-imidazole hydrochloride (**5c**). Following the general procedure, **4c** (2.93 mmol, 815 mg), HCl 2 M (29 mL) and ethereal HCl 2 M (2.0 mL) gave **5c** (702 mg, 96%) as a white solid. IR (ATR) 3349, 3089, 2731, 1614, 1492, 1269, 1151, 1110, 1023, 842, 773, 709 cm⁻¹. ¹H NMR (400 MHz, DMSO-*d*₆) δ 3.86 (s, 3H), 7.02 (dd, *J* = 8.5, 2.0 Hz, 1H), 7.23 (s, 1H), 7.74 (d, *J* = 8.5 Hz, 1H), 7.77 (s, 2H), 8.06 (s, 1H). ¹³C NMR (100.6 MHz) δ 55.9, 95.8, 110.2, 113.8, 120.2, 120.4 (2C), 123.2, 135.2, 139.6, 156.0, 159.8. HRMS C₁₂H₁₁N₂O₂ [M+H]⁺ 215.0815; found, 215.0814. Purity 99.6% (t_R = 3.20 min).

4.1.5.4. 2-(5-Bromobenzofuran-2-yl)-1H-imidazole hydrochloride (**5d**). Following the general procedure, **4d** (1.99 mmol, 650 mg), HCl 2 M (20 mL) and ethereal HCl 2 M (1.3 mL) gave **5d** (536 mg, 82%) as a white solid. IR (ATR) 3379, 3171, 2703, 1650, 1566, 1447, 1143, 1047, 879, 749, 718 cm⁻¹. ¹H NMR (400 MHz, DMSO-*d*₆) δ 7.62 (dd, *J* = 9.0, 2.0 Hz, 1H), 7.70 (d, *J* = 9.0 Hz, 1H), 7.83 (s, 2H), 8.07 (s, 1H), 8.12 (d, *J* = 2.0 Hz, 1H). ¹³C NMR (100.6 MHz) δ 108.9, 113.7, 116.6, 121.1 (2C), 125.3, 129.4, 129.8, 134.6, 142.0, 153.3. HRMS C₁₁H₈BrN₂O [M+H]⁺ 262.9815; found, 262.9813. Purity 98.6% (t_R = 3.47 min).

4.1.6. General procedure for the synthesis of 1-alkyl-2-(benzofuran-2-yl)-1H-imidazole hydrochlorides **6b** and **6c**

2-(Benzofuran-2-yl)-1H-imidazole hydrochlorides derivatives were neutralized with NaOH 2 N and the free base was extracted with AcOEt. The combined organic phases were washed with brine, dried over Na₂SO₄, and evaporated to give the desired amine. To a solution of the free base (1 equiv) generated from the corresponding 2-(benzofuran-2-yl)-1H-imidazole hydrochloride was treated with HBr 47% acid solution (0.5 mL) and the mixture was stirred at 100 °C for 7 h. After cooling the resulting solid was filtered, dissolved in water and basified with saturated NaHCO₃ solution. The free base was extracted with AcOEt. The combined organic phases were washed with brine, dried over Na₂SO₄, and evaporated to give a residue which was dissolved in diethyl ether/ethanol. Ethereal HCl 2 M (1.5 mmol/mL) was added and the precipitated salt was collected by filtration and was crystallized with acetonitrile.

4.1.6.1. 2-(5-Hydroxybenzofuran-2-yl)-1H-imidazole hydrochloride (**6b**). Following the general procedure, **5b** (0.93 mmol, 200 mg), HBr 47% acid solution (2 mL) and ethereal HCl 2 M (0.6 mL) gave **6b** (191 mg, 81%) as a yellowish solid. IR (ATR) 3266, 3009, 2819, 2731, 1593, 1443, 1370, 1246, 1195, 1157, 1090, 850, 802, 700 cm⁻¹. ¹H NMR (400 MHz, DMSO-*d*₆) δ 6.99 (dd, *J* = 9.0, 2.0 Hz, 1H), 7.14 (d, *J* = 2.0 Hz, 1H), 7.51 (d, *J* = 9.0 Hz, 1H), 7.80 (s, 2H), 7.97 (d, *J* = 1.0 Hz, 1H). ¹³C NMR (100.6 MHz) δ 106.4, 109.9, 111.9, 116.7, 120.6 (2C), 127.9, 135.2, 140.7, 148.9, 154.5. HRMS C₁₁H₉N₂O₂ [M+H]⁺

201.0659; found, 201.0656. Purity 98.1% ($t_R = 2.92$ min).

4.1.6.2. 2-(6-Hydroxybenzofuran-2-yl)-1H-imidazole hydrochloride (6c). Following the general procedure, **5c** (0.93 mmol, 200 mg), HBr 47% acid solution (1.9 mL) and ethereal HCl 2 M (0.6 mL) gave **6c** (183 mg, 77%) as a yellowish solid. IR (ATR) 3388, 3092, 2813, 2755, 1624, 1430, 1377, 1283, 1150, 1122, 1096, 839, 766, 708 cm^{-1} . ^1H NMR (400 MHz, DMSO- d_6) δ 6.92 (dd, $J = 8.5, 2.0$ Hz, 1H), 7.10 (s, 1H), 7.63 (d, $J = 8.5$ Hz, 1H), 7.77 (s, 2H), 8.01 (s, 1H), 10.30 (br s, 1H). ^{13}C NMR (100.6 MHz) δ 97.5, 110.6, 114.4, 118.9, 120.2 (2C), 123.2, 135.4, 138.7, 156.2, 158.4. HRMS $\text{C}_{11}\text{H}_9\text{N}_2\text{O}_2$ $[\text{M}+\text{H}]^+$ 201.0659; found, 201.0657. Purity 97.6% ($t_R = 2.91$ min).

4.1.7. General procedure for the synthesis of 1-alkyl-2-(benzofuran-2-yl)-1H-imidazole hydrochlorides **7a**, **7aa**, **7b** and **7c**

2-(Benzofuran-2-yl)-1H-imidazole hydrochlorides derivatives were neutralized with NaOH 2 N and the free base was extracted with AcOEt. The combined organic phases were washed with brine, dried over Na_2SO_4 , and evaporated to give the desired amine. To a solution of the free base (1 equiv) generated from the corresponding 2-(benzofuran-2-yl)-1H-imidazole hydrochloride in DMF (0.34 mmol/mL) at 0 °C was added sodium hydride (1.5 equiv, 60% in mineral oil). After 30 min at rt, methyl iodide/ethyl bromide (1.1 equiv) was added dropwise over 15 min at 0 °C. Then, the mixture was stirred for 30 min at rt, poured into water and extracted with AcOEt. The organic layer was washed with and the product was extracted with HCl 1 M. The aqueous layer was basified with NaOH 2 M and the free base was extracted with AcOEt. The combined organic phases were washed with brine, dried over Na_2SO_4 , and evaporated to give a residue which was dissolved in diethyl ether/ethanol. Ethereal HCl 2 M (1.5 mmol/mL) was added and the precipitated salt was collected by filtration and was crystallized with acetonitrile.

4.1.7.1. 1-Methyl-2-(benzofuran-2-yl)-1H-imidazole hydrochloride (7a). Following the general procedure, **LSL60101** (0.76 mmol, 140 mg), methyl iodide (0.84 mmol, 0.05 mL), sodium hydride 60% in mineral oil (1.14 mmol, 45.8 mg), DMF (2.3 mL) and ethereal HCl 2 M (0.5 mL) gave **7a** (150 mg, 84%) as a white solid. IR (ATR) 3306, 3095, 2569, 1634, 1445, 1270, 1188, 1131, 1033, 883, 756, 708 cm^{-1} . ^1H NMR (400 MHz, DMSO- d_6) δ 4.13 (s, 3H), 7.43 (t, $J = 7.5$ Hz, 1H), 7.55 (t, $J = 8.5$ Hz, 1H), 7.77 (d, $J = 8.5$ Hz, 1H), 7.80 (d, $J = 2.0$ Hz, 1H), 7.86–7.91 (m, 2H), 8.01 (s, 1H). ^{13}C NMR (100.6 MHz) δ 36.8, 111.5, 112.2, 121.0, 123.2, 124.9, 126.0, 127.4, 127.9, 135.6, 140.5, 154.9. HRMS $\text{C}_{12}\text{H}_{11}\text{N}_2\text{O}$ $[\text{M}+\text{H}]^+$ 199.0866; found, 199.0866. Purity 99.7% ($t_R = 3.15$ min).

4.1.7.2. 1-Ethyl-2-(benzofuran-2-yl)-1H-imidazole hydrochloride (7aa). Following the general procedure, **LSL60101** (1.36 mmol, 250 mg), ethyl bromide (1.42 mmol, 0.10 mL), sodium hydride 60% in mineral oil (2.04 mmol, 82 mg), DMF (4.0 mL) and ethereal HCl 2 M (0.9 mL) gave **7aa** (310 mg, 92%) as a white solid. IR (ATR) 3394, 3104, 2618, 1628, 1428, 1266, 1177, 1111, 929, 836, 761, 708 cm^{-1} . ^1H NMR (400 MHz, DMSO- d_6) δ 1.50 (t, $J = 7.0$ Hz, 3H), 4.55 (q, $J = 7.0$ Hz, 2H), 7.41 (d, $J = 7.5$ Hz, 1H), 7.53 (t, $J = 8.0$ Hz, 1H), 7.76 (d, $J = 8.5$ Hz, 1H), 7.86–7.88 (m, 2H), 8.00 (d, $J = 1.5$ Hz, 1H), 8.12 (s, 1H). ^{13}C NMR (100.6 MHz) δ 15.2, 44.3, 111.6, 111.8, 120.8, 122.8, 123.9, 124.5, 126.8, 127.5, 134.1, 139.7, 154.6. HRMS $\text{C}_{13}\text{H}_{13}\text{N}_2\text{O}$ $[\text{M}+\text{H}]^+$ 213.1022; found, 213.1021. Purity 100% ($t_R = 3.35$ min).

4.1.7.3. 1-Ethyl-2-(5-methoxybenzofuran-2-yl)-1H-imidazole hydrochloride (7b). Following the general procedure, **5b** (0.93 mmol, 200 mg), ethyl bromide (0.98 mmol, 0.07 mL), sodium hydride 60% in mineral oil (1.40 mmol, 56 mg), DMF (3 mL) and ethereal HCl 2 M (0.6 mL) gave **7b** (220 mg, 90%) as a white solid. IR (ATR) 3410, 3143,

2532, 1610, 1490, 1420, 1255, 1209, 1021, 928, 810, 758, 709 cm^{-1} . ^1H NMR (400 MHz, DMSO- d_6) δ 1.49 (t, $J = 7.0$ Hz, 3H), 3.82 (s, 3H), 4.54 (q, $J = 7.0$ Hz, 2H), 7.10 (dd, $J = 9.0, 2.5$ Hz, 1H), 7.35 (d, $J = 2.5$ Hz, 1H), 7.66 (d, $J = 9.0$ Hz, 1H), 7.85 (d, $J = 2.0$ Hz, 1H), 7.98 (d, $J = 2.0$ Hz, 1H), 8.06 (s, 1H). ^{13}C NMR (100.6 MHz) δ 15.2, 44.3, 55.7, 104.1, 111.7, 112.5, 116.8, 120.7, 123.8, 127.5, 134.1, 140.3, 149.6, 156.5. HRMS $\text{C}_{14}\text{H}_{15}\text{N}_2\text{O}_2$ $[\text{M}+\text{H}]^+$ 243.1128; found, 243.1128. Purity 98.4% ($t_R = 3.44$ min).

4.1.7.4. 1-Ethyl-2-(6-methoxybenzofuran-2-yl)-1H-imidazole hydrochloride (7c). Following the general procedure, **5c** (0.93 mmol, 200 mg), ethyl bromide (0.98 mmol, 0.07 mL), sodium hydride 60% in mineral oil (1.40 mmol, 56 mg), DMF (2.7 mL) and ethereal HCl 2 M (0.6 mL) gave **7c** (212 mg, 87%) as a white solid. IR (ATR) 3474, 3151, 2728, 1614, 1495, 1417, 1276, 1150, 1108, 1021, 928, 853, 813, 778, 701 cm^{-1} . ^1H NMR (400 MHz, DMSO- d_6) δ 1.49 (t, $J = 7.0$ Hz, 3H), 3.86 (s, 3H), 4.52 (q, $J = 7.0$ Hz, 2H), 7.03 (dd, $J = 8.5, 2.0$ Hz, 1H), 7.33 (s, 1H), 7.73 (d, $J = 8.5$ Hz, 1H), 7.82 (d, $J = 2.0$ Hz, 1H), 7.95 (d, $J = 2.0$ Hz, 1H), 8.05 (s, 1H). ^{13}C NMR (100.6 MHz) δ 15.2, 44.2, 55.9, 95.8, 112.0, 114.2, 119.9, 120.3, 123.1, 123.6, 134.3, 138.6, 156.1, 159.9. HRMS $\text{C}_{14}\text{H}_{15}\text{N}_2\text{O}_2$ $[\text{M}+\text{H}]^+$ 243.1128; found, 243.1128. Purity 99.2% ($t_R = 3.37$ min).

4.2. X-ray crystallographic analysis

Crystals of **LSL60101** were obtained from slow evaporation of methanol solutions. The single crystal X-Ray diffraction data set was collected at 294 K up to a max 2θ of ca. 57° on a Bruker Smart APEX II diffractometer, using monochromatic $\text{MoK}\alpha$ radiation $\lambda = 0.71073$ Å and 0.3° separation between frames. Data integration was performed using SAINT V6.45A and SORTAV (Blessing, 1995) in the diffractometer package. The crystal and collection data and structural refinement parameters are given in Table S14. The structure was solved by direct methods using SHELXT-2014 (Sheldrick, 2014) and Fourier's difference methods, and refined by least squares on F^2 using SHELXL-2014/7 (Sheldrick, 2014) inside the WinGX program environment (Farrugia, 2012). Atom coordinates are given in Table S15 and bond distances and angles in Table S16. The crystal structure shows the chlorohydrate form of **LSL60101**, which is as almost planar, as well as a methanol solvent molecule. Anisotropic displacement parameters were used for non-H atoms (Table S17) and the H-atoms were positioned in calculated positions (except H2) and refined riding on their parent atoms. Fig. 8 exhibits an ORTEP view of the molecule with the atom labelling, as well as its closest intermolecular bonds (Table S18) with the chloride anion (N12–H12...Cl1) and the methanol molecule (N9–H9...O2). These two intermolecular bonds are slightly out of the plane of the **LSL60101** molecule, producing a small torsion of the imidazolium group respect to the molecular mean plane ($\tau(\text{O1}–\text{C2}–\text{C8}–\text{N9}) = -4.3(11)$, $\tau(\text{C3}–\text{C2}–\text{C8}–\text{N12}) = -1.8(14)^\circ$). Methanol is also bonded to the chloride anion through the contact $\text{O2}–\text{H2}\cdots\text{Cl1}^i$ ($i = x-1, y, z$), giving rise to corrugated chains along **a**, assembled by parallel stacking along **c**. Crystallographic data (excluding structure factors) for the reported structure has been deposited in the Cambridge Crystallographic Data Centre as supplementary publication, CCDC No. 2063533. Copies of this information may be obtained free of charge from The Director, CCDC, 12 Union Road, Cambridge CB2 1EZ, UK. Fax: +44 1223 336 033. E-mail: data_request@ccdc.cam.ac.uk. Web page: <http://www.ccdc.cam.ac.uk>.

4.3. Binding studies

4.3.1. Preparation of cellular membranes

Male Swiss mice (final age 8–10 weeks) were killed, and the

brain cortex dissected and stored at -70°C until assays were performed. All animal experimental protocols were performed in agreement with European Union regulations (O.J. of E.C. L 358/1 18/12/1986).

Human brain samples were obtained at autopsy in the Basque Institute of Legal Medicine, Bilbao, Spain. Samples from the prefrontal cortex (Brodmann's area 9) were dissected at the time of autopsy and immediately stored at -70°C until assay. The study was developed in compliance with policies of research and ethical review boards for postmortem brain studies.

To obtain cellular membranes (P2 fraction) the different samples were homogenized using an ultraturrax in 10 vol of homogenization buffer (0.25 M sucrose, 5 mM Tris-HCl, pH 7.4). The crude homogenate was centrifuged for 5 min at 1000 g (4°C) and the supernatant was centrifuged again for 10 min at 40,000 g (4°C). The resultant pellet was washed twice in 5 vol of homogenization buffer and re-centrifuged in similar conditions. Protein content was measured according to the method of Bradford using BSA as standard.

4.3.2. Competition binding assays

The pharmacological activity of the compounds was evaluated through competition binding studies against the I_2 -IR selective radioligand [^3H]2-BFI or the α_2 -adrenergic receptor selective radioligand [^3H]RX821002. Specific binding was measured in 0.25 mL aliquots (50 mM Tris-HCl, pH 7.5) containing 100 μg of membranes, which were incubated in 96-well plates either with [^3H]2-BFI (2 nM) for 45 min at 25°C or [^3H]RX821002 (1 nM) for 30 min at 25°C , in the absence or presence of the competing compounds (10^{-12} to 10^{-3} M, 10 concentrations).

Specific binding of [^3H]clonidine (20 nM) to rat or human hypothalamic membranes pre-incubated with benextramine (100 μM) to alkylate the population of α_2 -adrenoceptors. Under these experimental conditions [^3H]clonidine only labelled I_1 -sites. In drug competition experiments, moxonidine (the reference compound for I_1 -IR) showed sub-nanomolar affinity for these I_1 -sites ($K_{\text{IH}} = 0.2$ nM; $K_{\text{IL}} = 32$ nM).

Incubations were terminated by separating free ligand from

bound ligand by rapid filtration under vacuum (1450 Filter Mate Harvester, PerkinElmer) through GF/C glass fiber filters. The filters were then rinsed three times with 300 μL of binding buffer, air-dried (120 min), and counted for radioactivity by liquid scintillation spectrometry using a MicroBeta TriLux counter (PerkinElmer). Specific binding was determined and plotted as a function of the compound concentration. Nonspecific binding was determined in the presence of idazoxan (10^{-5} M), a compound with well established affinity for I_2 -IR and α_2 -adrenergic receptors, in [^3H]2-BFI and [^3H]RX821002 assays. To obtain the inhibition constant (K_i) analyses of competition experiments were performed by nonlinear regression using the GraphPad Prism program. K_i values were normalized to $\text{p}K_i$ values. I_2 -IR/ α_2 selectivity index was calculated as the antilogarithm of the difference between $\text{p}K_i$ values for I_2 -IR and $\text{p}K_i$ values for α_2 -AR.

4.4. Acute toxicity

Lethal dose (LD_{50}) is a statistical derived amount of a compound that can be expected to cause death in 50% of the animals, rodents in general and is used as a measure of its acute toxicity. In this particular study, LD_{50} was calculated using the Logarithmic-Probit method, as initially described in Miller and Tainter (1944) [58], and the calculations further elaborated by Randhawa (2009) [59]. Male albino mice were administered i.p. with LSL60101 at a range of doses (10–100 mg/kg; $n = 10$ mice per dose tested), percentage mortalities were transformed to probits for each dose, and log-doses vs. probits were plotted to calculate LD_{50} (see further details in Ref. [59]).

4.5. 3D-QSAR study. Data set preparation

The original data set was divided on training set, that was used for model building and test set, used for model evaluation. The I_2 -IR 3D-QSAR model contains 24 compounds (Fig. S1), with 16 compounds in the training set and 8 compounds in the test set, while data set for the α_2 -AR 3D-QSAR model contains 22 compounds, with 14 compounds in the training set and 8 compounds in the test set (Tables S1 and S2). In order to compare and validate our results, we added three I_2 -IR standard ligands (tracizoline, idazoxan, and BU99008, Fig. 1), in both data sets. Test set compounds were chosen based on PCA (Principal Component Analysis) plot, considering that $\text{p}K_i$ values were homogeneously distributed in the whole range.

After dividing all data sets into training and test sets, variable selection was performed using fractional factorial design (FFD), and Partial Least Square (PLS) regression was applied for building 3D-QSAR models (Figs. S2 and S3).

Dominant forms of ligands at physiological pH 7.4 were obtained with the Marvin Sketch 5.5.1.0 program [60], while geometry was optimized with semiempirical/PM3 (Parameterized Model revision 3) method [61,62] followed by ab initio Hartree-Fock/3-21G method [63] using Gaussian 09 software [64] included in ChemBio3D Ultra 13 program [65].

The Pentacle program [38] was used for calculation of GRID independent descriptors (GRIND and GRIND2) and 3D-QSAR model building. Computation of descriptors is based on Molecular Interaction Fields (MIF), by using four different probes: O probe (hydrogen bond acceptor groups), N1 probe (hydrogen bond donor groups), TIP probe (the shape of molecule), and DRY probe (hydrophobic interactions). After MIFs calculation, ALMOND algorithm was used for the extraction of the most relevant regions, which represented the positions of favourable interactions between the ligand and probe. In the final step, Consistently Large Auto and Cross Correlation (CLACC) algorithm was used to plot node-node energies, between the same or a different probe, into auto- and

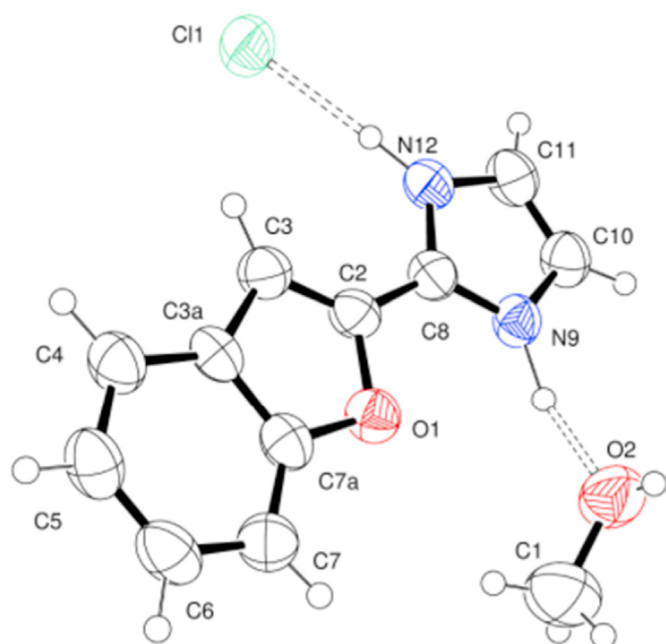


Fig. 8. X-ray crystal structure of LSL60101.

cross-correlograms, with the smoothing window set to 0.8 Å [66].

4.6. Cytotoxicity assays

Cancer cell lines LN-229, Capan-1, HCT-116, NCI-H460, HL-60, K-562 and Z-138 were acquired from the American Type Culture Collection (ATCC, Manassas, VA, USA) and the DND-41 cell line was purchased from the Deutsche Sammlung von Mikroorganismen und Zellkulturen (DSMZ Leibniz-Institut, Germany). All cell lines were cultured as recommended by the suppliers. Adherent cell lines LN-229, Capan-1, HCT-116 and NCI-H460 were seeded at a density between 500 and 1500 cells per well, in 384-well tissue culture plates (Greiner). After overnight incubation, cells were treated with different concentrations of the test compounds. Suspension cell lines HL-60, K-562, Z-138 and DND-41 were seeded at densities ranging from 2500 to 5500 cells per well in 384-well culture plates containing the test compounds at the same concentration points. The plates were incubated and monitored at 37 °C for 72 h in an IncuCyte® (Essen BioScience Inc., Sartorius) for real-time imaging of cell proliferation. Brightfield images were taken every 3 h, with one field imaged per well under 10x magnification. Cell growth was then quantified based on the percent cellular confluence as analysed by the IncuCyte® image analysis software, and used to calculate CC₅₀ values by linear interpolation.

4.7. Pharmacokinetic analysis and analysis conditions

The pharmacokinetic study was carried on in male CD1 mice (Envigo Laboratories) with a body weight between 40 and 50 g (n = 3–4 per group). Animals were randomized to be included in the treated or control groups. A single intraperitoneal dose of **LSL60101** (10 mg/kg, 10 ml/kg) was administered early in the morning (between 8 and 11 a.m.) without anaesthesia. Compound was dissolved in 10% of 2-hydroxypropyl-β-cyclodextrin in physiological saline). Mice were monitored for signs of pain or distress during the time between injection and euthanasia. Mice were sacrificed by cervical dislocation and blood (0.6 mL) was collected at different time points (15 min, 30 min, 45 min, 60 min, 2 h, 3 h, 4 h, 5 h, 8 h and 24 h after injection) in tubes with serum gel and clotting activator (Sarstedt Micro tube 1.1 mL Z-Gel). Samples were centrifuged at 10,000 rpm for 10 min to obtain plasma and stored at –80 °C up to analysis of compound concentration by HPLC-UV. Experimental procedures were in line with the Directive 2010/63/EU and approved by the Institutional Animal Care and Generalitat de Catalunya (#10291, 1/28/2018).

LSL60101 plasma concentrations versus time curves for the mean of animals were analysed by a non-compartmental model based on statistical moment theory using the “PK Solutions” computer program. The pharmacokinetic parameters calculated were the area under the concentration vs time curve (AUC), calculated using the trapezoidal rule in the interval 0–24 h; the half-life (t_{1/2β}), determined as ln2/β, being β, calculated from the slope of the linear, least-squares regression line; the C_{max} and T_{max} were read directly from the mean concentration curves.

The HPLC system was a PerkinElmer LC (Perkin Elmer INC, Massachusetts, U.S.) consisting of a Flexar LC pump, a chromatography interface (NCI 900 network), a Flexar LC autosampler PE, and a Waters 2487 dual λ absorbance detector. The chromatographic column was a kromasil 100-5-C18 (4.0 × 200 mm-Teknokroma Analítica S.A. Sant Cugat, Spain). Flux was 0.8 ml/min and the mobile phase consisted in 0.05 M KH₂PO₄ (30%):acetonitrile (70%) in isocratic conditions. The elution time of **LSL60101** was 4.4 min, and it was detected at 290 nm. The assay had a range of 0.025–5 µg/mL. The calibration curves were constructed by plotting the peak area ratio of the analysed peak against the known concentrations.

4.8. In vivo studies in mice

Studies and procedures involving mouse brain dissection and extractions were approved by the respective Local Bioethical Committees (Universitat de les Illes Balears-CAIB and University of Barcelona-GenCat) and followed the ARRIVE [67] and standard ethical guidelines (European Communities Council Directive 2010/63/EU and Guidelines for the Care and Use of Mammals in Neuroscience and Behavioural Research, National Research Council 2003). All efforts were made to minimize the number of animals used and their suffering.

4.9. Hypothermia in naïve mice

This study was performed in male and female adult CD-1 mice bred and housed in the animal facility at the University of the Balearic Islands in standard cages in set environmental conditions (22 °C, 70% humidity, and 12 h light/dark cycle, lights on at 8:00 a.m.) with free access to a standard diet and tap water. Prior to any experimental procedures, mice were habituated to the experimenter by being handled and weighed for 2 days. Mice were treated with a single dose of **LSL60101** (1, 5, 10, 20, 30 or 50 mg/kg, i.p., n = 5 for treatment group) or vehicle (2 ml/kg of saline, i.p., n = 5), and changes in rectal temperature were measured by comparing basal values (before drug treatment) with that obtained 1, 2 and 3 h post-treatment by a rectal probe connected to a digital thermometer (Compact LCD display thermometer, SA880-1 M, RS, Corby, UK).

4.10. Western blot analysis for FADD protein in naïve mice

For evaluating FADD protein regulation, a subgroup of mice received a single dose of **LSL60101** (30 or 50 mg/kg, i.p., n = 7 for treatment group) or vehicle (2 ml/kg of saline, i.p., n = 6) and were sacrificed 1 h after treatment. The hippocampus was freshly dissected and kept at –80 °C until hippocampal sample proteins (40 µg) were separated by SDS-PAGE on 10% polyacrylamide minigels (Bio-Rad) and transferred onto nitrocellulose membranes by standard Western blot (Wb) procedures as described previously [21]. Membranes were incubated overnight with anti-FADD (H-181; sc-5559; Santa Cruz Biotechnology, Santa Cruz, CA), and following secondary antibody (anti-rabbit) incubation and ECL detection system (Amersham, Buckinghamshire, UK), proteins were visualized on autoradiographic films (Amersham ECL Hyperfilm). The amount of FADD protein in mice brain samples from different treatment groups was compared with that of vehicle-treated controls (100%) in the same gel by densitometric scanning (GS-800 Imaging Densitometer, Bio-Rad) of immunoreactive bands (integrated optical density, IOD). Each brain sample was quantified in 2–4 gels, and the mean value was used as a final estimate. Quantification of β-actin contents (clone AC-15; Ab, no. A1978; Sigma) was used as a house-keeping control (no differences between treatment groups, 15 µg per sample).

4.11. 5XFAD as an animal model of AD: pharmacological treatments

The 5XFAD is a double transgenic APP/PS1 that co-expresses five mutations of AD and presents robust oxidative levels [68]. 6-month-old female 5XFAD mice (n = 20) and wild type (Wt) mice (n = 20) were used to carry out the molecular analyses. The animals were randomly allocated into four experimental groups: Control 5XFAD and Wt, administered with vehicle (2-hydroxypropyl)-β-cyclodextrin 1.8%, and treated 5XFAD and Wt administered with **LSL60101** diluted in vehicle (1 mg/kg/day). Treatment length was 4 weeks. Water consumption was controlled each week and the I₂-IR

ligand concentration was adjusted accordingly to reach the precise dose. Animals had free access to food and water, and were kept under standard temperature conditions ($22 \pm 2^\circ\text{C}$) and 12 h: 12 h light-dark cycles (300 lux/0 lux).

4.12. Western blot analysis in 5xFAD and Wt mice

For subcellular fractionation, 150 μL of buffer A (10 mM HEPES pH 7.9, 10 mM KCl, 0.1 mM EDTA pH 8, 0.1 mM EGTA pH 8, 1 mM DTT, 1 mM PMSF, protease inhibitors) were added to each sample and incubated on ice for 15 min. After this time, the samples were homogenized with a tissue homogenizer, 12.5 μL Igepal 1% were added, and the each eppendorf was vortexed for 15 s. Following 30 s of full-speed centrifugation at 4°C , supernatants were collected (cytoplasmic fraction); 80 μL of buffer C (20 mM HEPES pH 7.9, 0.4 M NaCl, 1 mM EDTA pH 8, 0.1 mM EGTA pH 8, 20% Glycerol 1 mM DTT, 1 mM PMSF, protease inhibitors) was added to each pellet and incubated under agitation at 4°C for 15 min. Subsequently, samples were centrifuged for 10 min at full speed at 4°C . Supernatants were collected (nuclear fraction).

For Western blot analysis, aliquots of 20 μg of total hippocampal protein were used. Protein samples from mice ($n = 3\text{--}5$ per group) were separated by Sodium dodecyl sulphate-polyacrylamide gel electrophoresis (SDS-PAGE) (8–12%) and transferred onto (Polyvinylidene difluoride) PVDF membranes (Millipore). Afterward, membranes were blocked in 5% non-fat milk in 0.1% Tris-buffered saline - Tween20 (TBS-T) for 1 h at room temperature, followed by overnight incubation at 4°C with the primary antibodies listed in Table S12.

Membranes were washed and incubated with the corresponding secondary antibodies for 1 h at room temperature. Immunoreactive proteins were viewed with a chemiluminescence-based detection kit, following the manufacturer's protocol (ECL Kit; Millipore) and digital images were acquired using a ChemiDoc XRS + System (Bio-Rad). Semi-quantitative analyses were carried out using ImageLab software (Bio-Rad), and results were expressed in Arbitrary Units (AU), considering control protein levels as 100%. Protein loading was routinely monitored by immunodetection of Glyceraldehyde-3-phosphate dehydrogenase (GADPH) (Table S12).

4.13. RNA extraction and gene expression determination in 5xFAD and Wt mice

Total RNA isolation was carried out using TRIzol[®] reagent according to manufacturer's instructions. The yield, purity, and quality of RNA were determined spectrophotometrically with a NanoDrop[™] ND-1000 (Thermo Scientific) apparatus and an Agilent 2100B Bioanalyzer (Agilent Technologies). RNAs with 260/280 ratios and RIN higher than 1.9 and 7.5, respectively, were selected. Reverse Transcription-Polymerase Chain Reaction (RT-PCR) was performed as follows: 2 μg of messenger RNA (mRNA) was reverse-transcribed using the High Capacity cDNA Reverse Transcription Kit (Applied Biosystems). Real-time quantitative PCR (qPCR) from 24 mice of both strains ($n = 4\text{--}6$ per group) was used to quantify mRNA expression of OS and inflammatory genes.

SYBR[®] Green real-time PCR was performed on a Step One Plus Detection System (Applied-Biosystems) employing SYBR[®] Green PCR Master Mix (Applied-Biosystems). Each reaction mixture contained 6.75 μL of complementary DNA (cDNA) (which concentration was 2 μg), 0.75 μL of each primer (which concentration was 100 nM), and 6.75 μL of SYBR[®] Green PCR Master Mix (2X). Data were analysed utilizing the comparative Cycle threshold (Ct) method ($\Delta\Delta\text{Ct}$), where the housekeeping gene level was used to

normalize differences in sample loading and preparation. The primers sequences used in this study are presented in Supplementary Table S10b. Normalization of expression levels was performed with β -actin for SYBR[®] Green-based real-time PCR. Each sample was analysed in duplicate, and the results represent the n -fold difference of the transcript levels among different groups.

4.14. Statistical analysis for 5xFAD and Wt mice comparisons

The statistical analysis was conducted using the statistical software GraphPad Prism version 8. Data were expressed as the mean \pm Standard Error of the Mean (SEM). Means were compared with two-way ANOVAs, followed by Tukey-Kramer multiple comparisons post-hoc analysis. Statistical significance was considered when p -values were <0.05 . The statistical outliers were carried out with Grubbs' test and subsequently removed from the analysis.

Declaration of competing interest

The authors declare that they have no known competing financial interests or personal relationships that could have appeared to influence the work reported in this paper.

Acknowledgment

This work was supported by Ministerio de Ciencia, Innovación y Universidades, Agencia Estatal de Investigación (Spain, PID2019-107991RB-I00, PID2019-106285RB), the Basque Government (IT1211/19) and Generalitat de Catalunya (GC) (2017SGR106). The project leading to these results has received funding from "la Caixa" Foundation (ID 100010434) under agreement CI18-00002. This activity has received funding from the European Institute of Innovation and Technology (EIT). This body of the European Union receives support from the European Union's Horizon 2020 research and innovation programme. C.G.-F, F.V., C.E., S.R.-A., A.B., and M.P. Financial support was provided for F.V. (University of Barcelona, APIF_2017), S.R.-A. (Generalitat de Catalunya, 2018FI_B_00227), A.B. (Institute of Biomedicine UB_2018), J.A.G.-S. is a member emeritus of the Institut d'Estudis Catalans (Barcelona, Catalonia). E.H.-H. is supported by a predoctoral scholarship (FPI/2102/2018; Consejería de Innovación, Investigación y Turismo del Gobierno de las Islas Baleares y del Fondo Social Europeo). M.R., T.D., and K.N. kindly acknowledge the project funded by the Ministry of Science and Technological Development of the Republic of Serbia, Contract No. 451-03-68/2020-14/200161, and HORIZON 2020-COST-Action CA18133 ERNEST: European Research Network on Signal Transduction. E. M. acknowledges funding to Severo Ochoa: CEX2019-917S. M.I.L, A.L.M. and J.B. gratefully acknowledge support from Xunta de Galicia (ED431C 2018/21 and ED431G 2019/02) and European Regional Development Fund (ERDF).

The authors thanks Dr. Rossend Obach and Dr. Ángel Menargues (LASA Laboratorios and later Ipsen Pharma SA, Barcelona, Spain) for initially providing the compound **LSL60101**.

Appendix A. Supplementary data

Supplementary data to this article can be found online at <https://doi.org/10.1016/j.ejmech.2021.113540>.

References

- [1] P. Bousquet, J. Feldman, J. Schwartz, Central cardiovascular effects of alpha adrenergic drugs: differences between catecholamines and imidazolines,

- J. Pharmacol. Exp. Therapeut. 230 (1984) 232–236.
- [2] P. Bousquet, A. Hudson, J.A. García-Sevilla, J.X. Li, Imidazoline receptor system: the past, the present, and the future, *Pharmacol. Rev.* 72 (2020) 50–79.
 - [3] J.X. Li, Imidazoline I₂ receptors: an update, *Pharmacol. Ther.* 178 (2017) 48–56.
 - [4] J. García-Sevilla, P.V. Escribá, M. Sastre, C. Walzer, X. Busquets, G. Jaquet, D.J. Reis, J. Guimón, Immunodetection and quantitation of imidazoline receptor proteins in platelets of patients with major depression and in brains of suicide victims, *Arch. Gen. Psychiatr.* 53 (1996) 803–810.
 - [5] J.A. Lowry, J.T. Brown, Significance of the imidazoline receptors in toxicology, *Clin. Toxicol.* 52 (2014) 454–469.
 - [6] J.X. Li, Y. Zhang, Imidazoline I₂ receptors: target for new analgesics? *Eur. J. Pharmacol.* 658 (2011) 49–56.
 - [7] S. Regunathan, D.L. Feinstein, D.J. Reis, Anti-proliferative and anti-inflammatory actions of imidazoline agents. Are imidazoline receptors involved? *Ann. N. Y. Acad. Sci.* 881 (1999) 410–419.
 - [8] K.L. Smith, D.S. Jessop, D.P. Finn, Modulation of stress by imidazoline binding sites: implications for psychiatric disorders, *Stress* 12 (2009) 97–114.
 - [9] J.J. Meana, F. Barturen, I. Martín, J.A. García-Sevilla, Evidence of increased non-adrenoreceptor [³H]idazoxan binding sites in the frontal cortex of depressed suicide victims, *Biol. Psychiatr.* 34 (1993) 498–501.
 - [10] J. Ruiz, I. Martín, L.F. Callado, J.J. Meana, F. Barturen, J.A. García-Sevilla, Non-adrenoreceptor [³H]idazoxan binding sites (I₂-imidazoline sites) are increased in postmortem brain from patients with Alzheimer's disease, *Neurosci. Lett.* 160 (1993) 109–112.
 - [11] C. Gargalidis-Moudanos, N. Pizzinat, F. Javoy-Agud, A. Remaury, A. Parini, I₂-imidazoline binding sites and monoamine oxidase activity in human post-mortem brain from patients with Parkinson's disease, *Neurochem. Int.* 30 (1997) 31–36.
 - [12] L.F. Callado, J.I. Martín-Gómez, J. Ruiz, J.M. Garibi, J.J. Meana, Imidazoline I₂ receptors density increases with the malignancy of human gliomas, *J. Neurol. Neurosurg. Psychiatry* 75 (2004) 785–787.
 - [13] C. Dardonville, I. Rozas, Imidazoline binding sites and their ligands: an overview of the different chemical structures, *Med. Res. Rev.* 24 (2004) 639–661.
 - [14] G.M. Gilad, V.H. Gilad, Accelerated functional recovery and neuroprotection by agmatine after spinal cord ischemia in rats, *Neurosci. Lett.* 296 (2000) 97–100.
 - [15] K. Maiese, L. Pek, S.B. Berger, D.J. Reis, Reduction in focal cerebral ischemia by agents acting at imidazole receptors, *J. Cerebr. Blood Flow Metabol.* 12 (1992) 53–63.
 - [16] Z. Han, M.J. Xiao, B. Shao, R.Y. Zheng, G.Y. Yang, K. Jin, Attenuation of ischemia induced rat brain injury by 2-(2-benzofuranyl)-2-imidazoline, a high selectivity ligand for imidazoline (I₂) receptors, *Neurosci. Res.* 31 (2009) 390–395.
 - [17] S.X. Jiang, R.Y. Zheng, J.Q. Zheng, X.L. Li, Z. Han, S.T. Hou, Reversible inhibition of intracellular calcium influx through NMDA receptors by imidazoline (I₂) receptor antagonists, *Eur. J. Pharmacol.* 629 (2010) 12–19.
 - [18] L.C. Rovati, N. Brambilla, T. Blicharski, J. Connell, C. Vitalini, A. Bonazzi, G. Giacobelli, F. Girolami, M. D'Amato, Efficacy and safety of the first-in-class imidazoline-2 receptor ligand CR4056 in pain from knee osteoarthritis and disease phenotypes: a randomized, double-blind, placebo-controlled phase 2 trial, *Osteoarthritis Cartilage* 28 (2020) 22–30.
 - [19] R.J. Tyacke, J.F.M. Myers, A.V. Venkataraman, I. Mick, S. Turton, J. Passchier, S.M. Husband, E.A. Rabiner, R.N. Gunn, P.S. Murphy, C.A. Parker, D.J. Nutt, Evaluation of [¹¹C]-BU99008, a PET ligand for the imidazoline-2 binding site in human brain, *J. Nucl. Med.* 59 (2018) 1597–1602.
 - [20] H. Wilson, G. Dervenoulas, G. Pagano, R.J. Tyacke, S. Polychronis, J. Myers, R.N. Gunn, E.A. Rabiner, D. Nutt, M. Politis, Imidazoline 2 binding sites reflecting astroglia pathology in Parkinson's disease: an in vivo [¹¹C]-BU99008 PET study, *Brain* 10 (2019) 3116–3128.
 - [21] S. Abás, A.M. Erdozain, B. Keller, S. Rodríguez-Arévalo, L.F. Callado, J.A. García-Sevilla, C. Escolano, Neuroprotective effects of a structurally new family of high affinity imidazoline I₂ receptors ligands, *ACS Chem. Neurosci.* 8 (2017) 737–742.
 - [22] C. Grinán-Ferré, F. Vasilopoulou, S. Abás, S. Rodríguez-Arévalo, A. Bagán, F.X. Sureda, B. Pérez, L.F. Callado, J.A. García-Sevilla, M.J. García-Fuster, C. Escolano, M. Pallàs, Behavioral and cognitive improvement induced by novel imidazoline I₂ receptor ligands in female SAMP8 mice, *Neurotherapeutics* 16 (2019) 416–431.
 - [23] S. Abás, S. Rodríguez-Arévalo, A. Bagán, C. Grinán-Ferré, F. Vasilopoulou, I. Brocos-Mosquera, C. Muguiza, B. Pérez, E. Molins, F.J. Luque, P. Pérez-Lozano, S. de Jonghe, D. Daelemans, L. Naesens, J. Brea, M.I. Loza, E. Hernández-Hernández, J.A. García-Sevilla, M.J. García-Fuster, M. Radan, T. Djikic, K. Nikolic, M. Pallàs, L.F. Callado, C. Escolano, Bicyclic α -iminophosphonates as high affinity imidazoline I₂ receptor ligands for Alzheimer's disease, *J. Med. Chem.* 7 (2020) 3610–3633.
 - [24] D.A. Ruggiero, S. Regunathan, H. Wang, T.A. Milner, D.J. Reis, Immunocytochemical localization of an imidazoline receptor protein in the central nervous system, *Brain Res.* 780 (1998) 270–293.
 - [25] J.A. García-Sevilla, P.V. Escribá, C. Walzer, C. Bouras, J. Guimón, Imidazoline receptor proteins in brains of patients with Alzheimer's disease, *Neurosci. Lett.* 247 (1998) 95–98.
 - [26] D.S. Albers, M.F. Beal, Mitochondrial dysfunction and oxidative stress in aging and neurodegenerative diseases, *J. Neural. Transm. Suppl.* 5 (2000) 133–154.
 - [27] J.P. Bolaños, M.A. Moro, I. Lizasoain, A. Almeida, Mitochondrial and reactive oxygen and nitrogen species in neurological disorders and stroke: therapeutic implications, *Adv. Drug Deliv. Rev.* 61 (2009) 1299–1315.
 - [28] Z. Liu, T. Zhou, A.C. Ziegler, P. Dimitrion, L. Zuo, Oxidative stress in neurodegenerative diseases: from molecular mechanisms to clinical applications, *Oxid. Med. Cell Longev.* 2017 (2017) 1–11.
 - [29] M. Johnstone, A.J. Geraing, K.M. Miller, A central role for astrocytes in the inflammatory response to beta-amyloid: chemokines, cytokines and reactive oxygen species are produced, *J. Neuroimmunol.* 93 (1999) 182–193.
 - [30] D.J. Bonda, X. Wang, G. Perry, A. Nunomura, M. Tabaton, X. Zhu, M.A. Smith, Oxidative stress in Alzheimer disease: a possibility for prevention, *Neuropharmacology* 59 (2010) 290–294.
 - [31] L.A. Lione, D.J. Nutt, A.L. Hudson, Characterisation and localisation of [³H]-2-(2-benzofuranyl)-2-imidazoline binding in rat brain: a selective ligand for imidazoline I₂ receptors, *Eur. J. Pharmacol.* 353 (1998) 123–135.
 - [32] F. Vasilopoulou, C. Grinán-Ferré, S. Rodríguez-Arévalo, A. Bagán, S. Abás, C. Escolano, M. Pallàs, I₂ imidazoline receptor modulation protects aged SAMP8 mice against cognitive decline by suppressing the calcineurin pathway, *GeroScience* 43 (2021) 965–983.
 - [33] J.A. García-Sevilla, J.J. Meana, F. Barturen, F.A. Gejjo, A. Menargues, R. Obach, F. Pla, Benzofuranylimidazole Derivatives and Therapeutical Compositions Containing the Same, 1994. US5354769(A), October 11.
 - [34] R. Alemany, G. Olmos, P.V. Escribá, A. Menargues, R. Obach, J.A. García-Sevilla, LSL60101, a selective ligand for imidazoline I₂ receptors, on glial fibrillary acidic protein concentration, *Eur. J. Pharmacol.* 280 (1995) 205–210.
 - [35] M.A. Boronat, G. Olmos, J.A. García-Sevilla, Attenuation of tolerance to opioid-induced antinociception and protection against morphine-induced decrease of neurofilament proteins by idazoxan and other I₂-imidazoline ligands, *Br. J. Pharmacol.* 125 (1998) 175–185.
 - [36] A. Casanova, G. Olmos, J. Ribera, M.A. Boronat, J.E. Esquerda, J.A. García-Sevilla, Induction of reactive astrocytosis and prevention of motoneuron cell death by the I₂-imidazoline receptor ligand LSL60101, *Br. J. Pharmacol.* 130 (2000) 1767–1776.
 - [37] N. MacInnes, S.L. Handley, Characterization of the discriminable stimulus produced by 2-BFI: effects of imidazoline I₂-site ligands, MAOIs, β -carbolines, agmatine and ibogaine, *Br. J. Pharmacol.* 135 (2002) 1227–1234.
 - [38] Pentacle, Version 1.0.6, MolecularDiscoveryLtd., Perugia, Italy, 2009.
 - [39] A. Krüger, V. Gonçalves, C. Wrenger, T. Kronenberger, ADME Profiling in Drug Discovery and a New Path Paved on Silica, *Drug Discovery and Development - New Advances*, 2019.
 - [40] ADMET Predictor, V. 9.5, Simulations Plus Inc., Lancaster, CA, USA. <https://www.simulations-plus.com>.
 - [41] A. Daina, O. Michielin, V. Zoete, SwissADME: a free web tool to evaluate pharmacokinetics, drug-likeness and medicinal chemistry friendliness of small mol, *Sci. Rep.* 7 (2017) 1–13.
 - [42] D.A. Thorn, X. An, Y. Zhang, M. Pignini, J. Li, Characterization of the hypothermic effects of imidazoline I₂ receptor agonists in rats, *Br. J. Pharmacol.* 166 (2012) 1936–1945.
 - [43] E. Hernández-Hernández, M.J. García-Fuster, Evaluating the effects of 2-BFI and trazoline, two potent I₂-imidazoline receptor agonists, on cognitive performance and affect in middle-aged rats, *Naunyn-Schmiedeberg's Arch. Pharmacol. Pharmacology* 394 (2021) 989–996.
 - [44] J.A. Craven, E.L. Conway, Effects of alpha 2-adrenoceptor antagonists and imidazoline 2-receptor ligands on neuronal damage in global ischemia in the rat, *Clin. Exp. Pharmacol. Physiol.* 24 (1997) 204–207.
 - [45] D.W. Marion, L.E. Penrod, S.F. Kelsey, W.D. Obrist, P.M. Kochanek, A.M. Palmer, S.R. Wisniewski, S.T. DeKosky, Treatment of traumatic brain injury with moderate hypothermia, *N. Engl. J. Med.* 336 (1997) 540–546.
 - [46] C.M. Maier, K.V. Ahern, M.L. Cheng, J.E. Lee, M.A. Yenari, G.K. Steinberg, J.R. Kirsch, Optimal depth and duration of mild hypothermia in a focal model of transient cerebral ischemia: effects on neurologic outcome, infarct size, apoptosis, and inflammation, *Stroke* 29 (10) (1998) 2171–2180.
 - [47] E. Hernández-Hernández, A. Miralles, S. Esteban, M.J. García-Fuster, Improved age-related deficits in cognitive performance and affective-like behavior following acute, but not repeated, 8-OH-DPAT treatments in rats: regulation of hippocampal FADD, *Neurobiol. Aging* 71 (2018) 115–126.
 - [48] E. Hernández-Hernández, A. Miralles, S. Esteban, M.J. García-Fuster, Repeated treatment with the α 2-adrenoceptor agonist UK-14304 improves cognitive performance in middle-age rats: role of hippocampal Fas-associated death domain, *J. Psychopharmacol.* 32 (2) (2018) 248–255.
 - [49] E. Comi, M. Lanza, F. Ferrari, V. Mauri, G. Caselli, L.C. Rovati, Efficacy of CR4056, a first-in-class imidazoline-2 analgesic drug, in comparison with naproxen in two rat models of osteoarthritis, *J. Pain Res.* 10 (2017) 1033–1043.
 - [50] N. Mirzaei, B.C. Mota, A.M. Birch, N. Davis, C. Romero-Molina, L. Katsouri, E.O.C. Palmer, A. Golbano, L.J. Riggall, I. Nagy, R. Tyacke, D.J. Nutt, M. Sastre, Imidazoline ligand BU224 reverses cognitive deficits, reduces microgliosis and enhances synaptic connectivity in a mouse model of Alzheimer's disease, *Br. J. Pharmacol.* 178 (3) (2021) 654–671.
 - [51] J.A. García-Sevilla, P.V. Escribá, C. Walzer, C. Bouras, J. Guimón, Imidazoline receptor proteins in brains of patients with Alzheimer's disease, *Neurosci. Lett.* 247 (1998) 95–98.
 - [52] B. Uttara, A.V. Singh, P. Zamboni, R.T. Mahajan, Oxidative stress and neurodegenerative diseases: a review of upstream and downstream antioxidant therapeutic options, *Curr. Neuropharmacol.* 7 (1) (2009) 65–74.
 - [53] E. Birben, U.M. Sahiner, C. Sackesen, S. Erzurum, O. Kalayci, Oxidative stress and antioxidant defense, *World Allergy Organ. J.* 5 (1) (2012) 9–19.
 - [54] J.S. Tian, Q.J. Zhai, Y. Zhao, R. Chen, L.D. Zhao, 2-(2-benzofuranyl)-2-imidazoline (2-BFI) improved the impairments in AD rat models by

- inhibiting oxidative stress, inflammation and apoptosis, *J. Integr. Neurosci.* 16 (4) (2017) 385–400.
- [55] D.H. Choi, J.H. Yun, J. Lee, Protective effect of the imidazoline I₂ receptor agonist 2-BFI on oxidative cytotoxicity in astrocytes, *Biochem. Biophys. Res. Commun.* 503 (4) (2018) 3011–3016.
- [56] F. Vasilopoulou, S. Rodríguez-Arévalo, A. Bagán, C. Escolano, C. Griñán-Ferré, M. Pallàs, Disease-modifying treatment with I₂ imidazoline receptor ligand LSL60101 in an Alzheimer's disease mouse model: a Comparative study with donepezil, *Br. J. Pharmacol.* (2021) 1–17.
- [57] Y. Chen, C. Qin, J. Huang, X. Tang, C. Liu, K. Huang, J. Xu, G. Guo, A. Tong, L. Zhou, The role of astrocytes in oxidative stress of central nervous system: a mixed blessing, *Cell Prolif* 53 (3) (2020) e12781.
- [58] L.C. Miller, M.L. Tainter, Estimation of the ED₅₀ and its error by means of logarithmic-probit graph paper, *Proc. Soc. Exp. Bio. Med.* 57 (1944) 261–264.
- [59] M.A. Randhawa, Calculation of LD₅₀ values from the method of miller and tainter, 1944, *J. Ayub Med. Coll. Abbottabad* 21 (3) (2009) 184–185.
- [60] MarvinSketch 5.5.1.0, ChemAxon, Budapest, Hungary, 2011 software available at, <https://www.chemaxon.com>.
- [61] J.J.P. Stewart, Optimization of parameters for semiempirical methods I. Method, *J. Comput. Chem.* 10 (1989) 209–220.
- [62] J.J.P. Stewart, Optimization of parameters for semiempirical methods II. Applications, *J. Comput. Chem.* 10 (1989) 221–264.
- [63] W.J. Hehre, L. Radom, P.V.R. Schleyer, J. Pople, *AB Initio Molecular Orbital Theory*, Wiley, 1986.
- [64] M.J. Frisch, *Gaussian 98 (Revision A.7)*, 1998.
- [65] CambridgeSoft Corporation, *ChemBio3D Ultra, Version 13.0*, 2013. Cambridge, MA, USA.
- [66] A. Duran, M. Pastor, An advanced tool for computing and handling grid-independent descriptors, *User Manual (2011)*. Version 1.06.
- [67] N. Percie du Sert, A. Ahluwalia, S. Alam, M.T. Avey, M. Baker, W.J. Browne, A. Clark, I.C. Cuthill, U. Dirnagl, M. Emerson, P. Garner, S.T. Holgate, D.W. Howells, V. Hurst, N.A. Karp, S.E. Lazic, K. Lidster, C.J. MacCallum, M. Macleod, E.J. Pearl, O.H. Petersen, F. Rawle, P. Reynolds, K. Rooney, E.S. Sena, S.D. Silberberg, T. Steckler, H. Würbel, Reporting animal research: explanation and elaboration for the ARRIVE guidelines 2.0, *PLoS Biol.* 18 (7) (2020), <https://doi.org/10.1371/journal.pbio.3000411>.
- [68] H. Oakley, S.L. Cole, S. Logan, E. Maus, P. Shao, J. Craft, A. Guillozet-Bongaarts, M. Ohno, J. Disterhoft, L. Van Eldik, R. Berry, R. Vassar, Intra-neuronal β -amyloid aggregates, neurodegeneration, and neuron loss in transgenic mice with five familial Alzheimer's disease mutations: potential factors in amyloid plaque formation, *J. Neurosci.* 26 (2006) 10129–10140.